

# Chapter 2

## Earth-Abundant $\text{Cu}_2\text{ZnSn}(\text{S},\text{Se})_4$ (CZTSSe) Solar Cells

Sandip Das, Krishna C. Mandal and Raghu N. Bhattacharya

### 2.1 Introduction

Current benchmark thin film solar cell (TFSC) technologies based on polycrystalline  $\text{CuIn}_x\text{Ga}_{1-x}\text{S}(\text{Se})_2$  (CIGS) and CdTe absorber materials have reached record efficiencies of 20.8 and 19.6 % for laboratory-scale devices and have already reached the commercial production stage [1]. However, these thin film photovoltaic (PV) technologies suffer from serious issues of toxicity, skyrocketing material cost, and/or low abundance of raw materials, which are predicted to severely limit the production, mass deployment, and economic sustainability of these solar cells [2–9]. Indium (In), gallium (Ga), and tellurium (Te) supply have been categorized as “critical” by the US Department of Energy (DOE) and the European Commission (EC) [10, 11]. Particularly, In supply for CIGS production could be stringent as more than 80 % of In produced worldwide is consumed by the flat panel display (FPD) industry and with ever-increasing demand of such displays, sustainability and economic viability of CIGS PV technology could be in great danger in upcoming years [12]. Also, due to the environmental health concerns, use of toxic cadmium (Cd) hinders the mass production and deployment of CdTe solar cells [13]. Thus, an intense research effort has been triggered to develop alternative thin film solar absorber materials comprising of earth-abundant, low-cost, and non-toxic elements which can yield high-efficiency devices, be economically

---

S. Das

Department of Electrical Engineering, Kennesaw State University,  
Marietta, GA 30060 USA

K.C. Mandal

Department of Electrical Engineering, University of South Carolina,  
Columbia, SC 29208 USA

R.N. Bhattacharya (✉)

National Renewable Energy Laboratory, Golden, CO 80401, USA  
e-mail: Raghu.Bhattacharya@nrel.gov

competitive with the conventional energy sources, and support terawatt (TW)-scale PV generation in the near future.

Copper (Cu)-based  $I_2-II-IV-VI_4$  quaternary kesterite compounds— $Cu_2ZnSnS_4$  (CZTS),  $Cu_2ZnSnSe_4$  (CZTSe), and mixed chalcogenide  $Cu_2ZnSn(S_xSe_{1-x})_4$  (CZTSSe) have emerged as the potential alternative to the existing CIGS and CdTe absorbers in thin film solar cells. CZTS(Se) is an attractive choice for thin film solar cell absorber material owing to its tunable direct bandgap of 1.0–1.5 eV with a large optical absorption coefficient ( $>10^4 \text{ cm}^{-1}$ ) and p-type conductivity [14–19]. The constituent elements of CZTS(Se) are earth abundant, inexpensive, and environmentally benign. The reserve of Cu, Zn, Sn, and sulfur on earth’s crust is 68 ppm, 79 ppm, 2.2 ppm, and 420 ppm, respectively, compared to 0.16 ppm of In, 0.15 ppm of Cd, and 0.001 ppm of Te [20].

The availability of Zn and Sn is about 500 and 14 times higher, and the annual global production is 20 times and 340 times more compared to the scarce and expensive In [21]. Also, the Zn price is nearly two orders and Sn price is one order of magnitude less than indium, while the In price is sharply rising [21, 22]. Abundance and recent cost of the constituent elements for CZTS(Se), CIGS, and CdTe compounds are illustrated in Fig. 2.1.

Calculations according to the Shockley–Queisser photon balance have estimated the theoretical conversion efficiency of single-junction CZTS(Se) solar cells to be as high as 32.2 % [23]. In light of the above-mentioned advantages, CZTS(Se) shows extreme promise to be the ideal thin film solar cell material for low-cost, sustainable, high-efficiency, and environment-friendly PV technology.

Significant developments have been made on CZTS(Se)-based thin film photovoltaic solar cells in the past few years, reporting solar cell with  $\sim 11$  % efficiency [24]. However, CZTS(Se) PV technology is currently in its amateur state and requires extensive research to become marketable in the near future. This

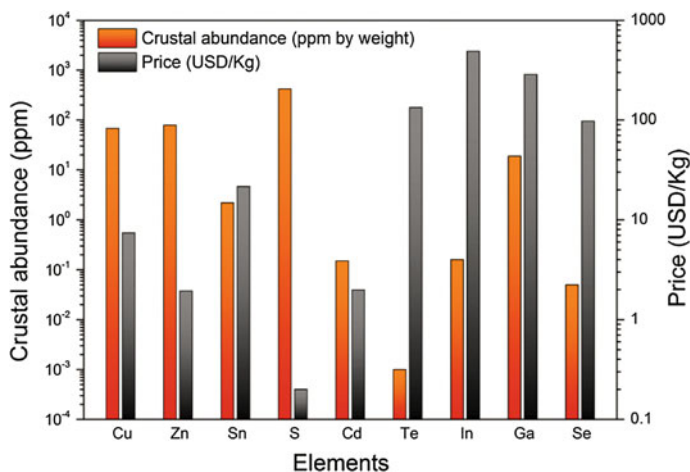


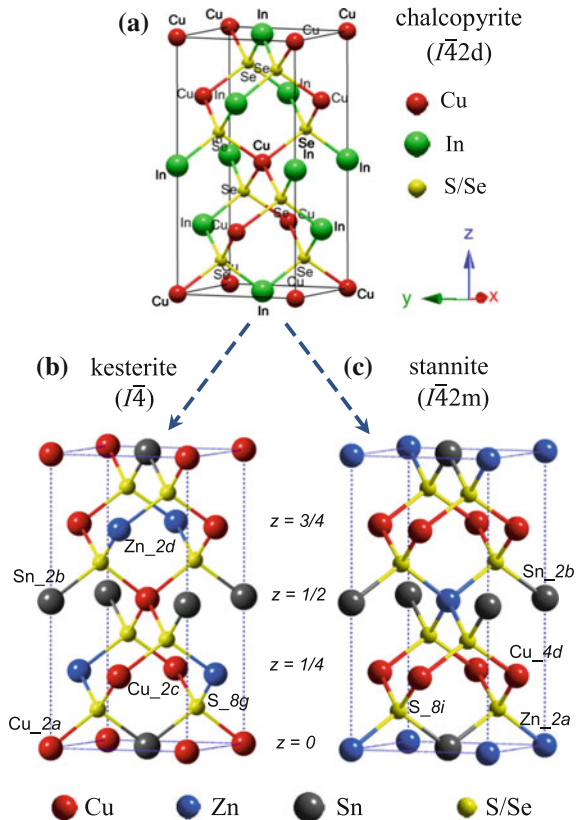
**Fig. 2.1** Abundance on earth’s crust and cost of constituent elements for CIGS, CdTe, and CZTS (Se) absorber materials for thin film solar cells

chapter presents an overview of the various techniques employed to prepare CZTS (Se) absorber material, physical properties of the material, defect physics, and photovoltaic performances of selected high-efficiency solar cells achieved following different absorber preparation routes.

## 2.2 Crystal Structure

$\text{Cu}_2\text{ZnSn}(\text{S},\text{Se})_4$  belongs to the  $\text{I}_2\text{-II-IV-VI}_4$  quaternary material system with similar structure to that of ternary chalcopyrite material  $\text{CuInSe}_2$  (space group  $\bar{1}\bar{4}2d$ ) (Fig. 2.2a), in which one half of In atoms (group III) are replaced by Zn (group II) and other half by Sn atoms (group IV).  $\text{Cu}_2\text{ZnSn}(\text{S},\text{Se})_4$  crystallizes in two primary crystalline structures known as kesterite (space group  $\bar{1}\bar{4}$ ) and stannite (space group  $\bar{1}\bar{4}2m$ ) [25–28]. These two crystal structures are very similar; both have cations located at tetrahedral sites but differ in the stacking arrangement of Cu and Zn atoms along the  $c$ -axis [26–31]. The crystal structure and atomic arrangements for the kesterite and stannite structures are illustrated in Fig. 2.2b and c, respectively.

**Fig. 2.2** Crystal structure of **a** chalcopyrite  $\text{CuInSe}_2$ , **b** kesterite  $\text{Cu}_2\text{ZnSnS}_4$ , and **c** stannite  $\text{Cu}_2\text{ZnSnS}_4$



In kesterite structure, the cationic layers along the  $c$ -axis are arranged in the Cu–Sn, Cu–Zn, Cu–Sn, and Cu–Zn fashion. One Cu atom is located at  $2a$  position; Zn atom and the other Cu atom are located at  $2d$  and  $2c$  positions, respectively, with corresponding Madelung potentials of  $-15.04$ ,  $-21.88$ , and  $-15.21$  V. In stannite structure, a periodic arrangement of Zn–Sn cationic layer sandwiched in between Cu–Cu layers is repeated, where both Cu atoms are located at  $4d$  position and the Zn atom at  $2a$  position with Madelung potentials of  $-15.30$  and  $-21.62$  V, respectively. Sn atom site is located at  $2b$  position in both structures [32, 33]. Theoretical studies have predicted that the kesterite phase has slightly lower energy compared to the stannite phase and therefore should be thermodynamically more stable than stannite counterpart [33–40]. As predicted theoretically, most of CZTS samples have been reported to have kesterite structure.

Due to the similar structural properties and isoelectronic nature of  $\text{Cu}^+$  and  $\text{Zn}^{2+}$ , it is very difficult to distinguish between the kesterite and stannite phases experimentally by X-ray diffraction. Recently, neutron diffraction [31] and anomalous diffusion [41] studies confirmed that  $\text{Cu}_2\text{ZnSn}(\text{S},\text{Se})_4$  compounds crystallize in kesterite structure and are dominant at temperature  $<876$  °C. It is suggested that observations of stannite structure for  $\text{Cu}_2\text{ZnSn}(\text{S},\text{Se})_4$  compounds were due to the existence of partial disorders of Cu and Zn sites in the I–II (001) layer of the kesterite phase [31, 42, 43]. This disorder could be due to the formation of both kesterite and stannite phases during crystallization process since there is only a negligible difference in the lattice parameters and the total energy.

## 2.3 Solar Cell Structure

The well-studied CIGS thin film solar cell structure is usually inherited for CZTS-based devices. The schematic structure of a typical CZTS solar cell is shown in Fig. 2.3a, and a corresponding cross-sectional SEM image showing the device

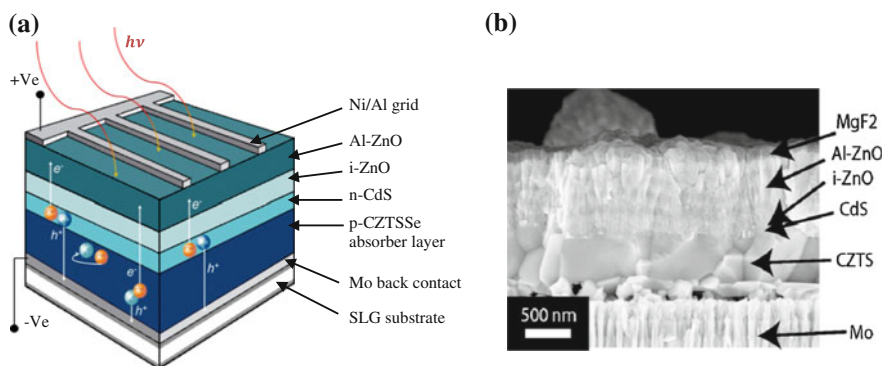


**Fig. 2.3** **a** Schematic device structure of a typical CZTSSe thin film solar cell, **b** cross-sectional SEM image showing all layers of the device [17]

structure is presented in Fig. 2.3b. Sputtered bilayer molybdenum (Mo) film with a thickness of  $\sim 0.5\text{--}1.0\ \mu\text{m}$  deposited on soda-lime glass (SLG) substrate is used as the standard back contact. The p-type CZTS absorber layer with thickness ranging from  $\sim 0.6$  to  $2.0\ \mu\text{m}$  is grown on the Mo film. A thin n-type CdS layer of  $50\text{--}100\ \text{nm}$  thickness is deposited on the p-CZTS film, usually by chemical bath deposition to fabricate the heterojunction. Subsequently, the device structure is completed by deposition of a  $50\text{--}90\text{-nm}$  high-resistive intrinsic ZnO (i-ZnO) buffer layer followed by the deposition of a transparent conducting oxide (TCO) layer as the front contact. Typically,  $0.5\text{--}1.0\ \mu\text{m}$  thick Al-doped n-type ZnO (Al-ZnO) or indium tin oxide (ITO) is used as the TCO. Finally, Ni/Al grid lines are deposited on the TCO layer for improved current collection. The typical device configuration of a CZTS-based solar cell is as follows: SLG/Mo/CZTS/CdS/i-ZnO/Al:ZnO/Al/Ni. In order to reduce the loss of reflection,  $\text{MgF}_2$  antireflection coating is often deposited on top of the cell to capture the incident light more efficiently.

## 2.4 Composition and Phase Diagram

It is extremely challenging to grow pure single-phase kesterite  $\text{Cu}_2\text{ZnSnS}(\text{Se})_4$ . CZTS(Se) can be grown via solid-state chemical reactions between  $\text{Cu}_2\text{S}$ ,  $\text{ZnS}$ , and  $\text{SnS}_2$  (or  $\text{Cu}_2\text{Se}$ ,  $\text{ZnSe}$ , and  $\text{SnSe}_2$ ). Due to the complexity of the quaternary material system, several binary and ternary sulfides (or selenides) including  $\text{Zn}_x\text{S}$  (Se),  $\text{Cu}_x\text{S}$  (Se),  $\text{Sn}_x\text{S}$  (Se), and  $\text{Cu}_x\text{SnS}(\text{Se})_y$  phases can easily form during the CZTS (Se) film growth which may adversely affect the photovoltaic performance of the resulting device. The ternary phase diagram of the  $\text{Cu}_2\text{S}\text{--ZnS}\text{--SnS}_2$  (or  $\text{Cu}_2\text{Se}\text{--ZnSe}\text{--SnSe}_2$ ) system exhibits very narrow region of stability for single-phase kesterite CZTS(Se) crystals (Fig. 2.4) [44–47]. Kesterite structure is highly sensitive to composition compared to the chalcopyrite structure [48–51]. Only 1–2 %

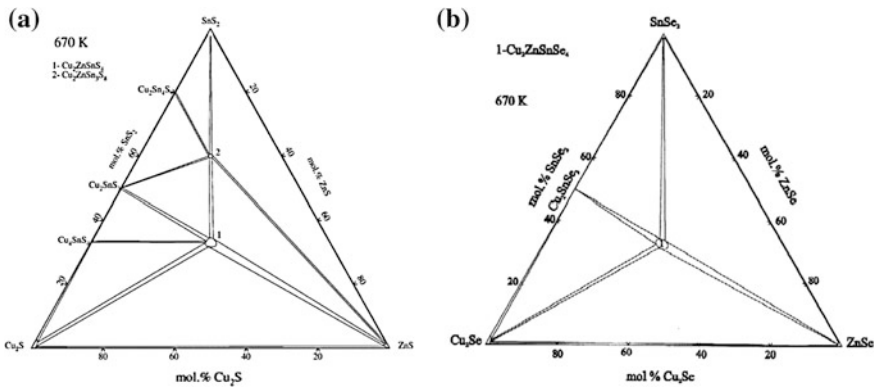


**Fig. 2.4** Phase diagrams of **a**  $\text{Cu}_2\text{S}\text{--ZnS}\text{--SnS}_2$  [44] and **b**  $\text{Cu}_2\text{Se}\text{--ZnSe}\text{--SnSe}_2$  pseudo-ternary systems at 670 K [45]

deviation from the ideal stoichiometric composition is allowed compared to  $\sim 4\%$  deviation in chalcopyrites [52]. Also, the stability region of  $\text{Cu}_2\text{ZnSnS}_4$  for Cu-rich condition in the chemical potential  $\mu_{\text{Sn}}-\mu_{\text{Zn}}$  diagram is about 0.1 eV wide stability region [48, 49, 53] compared to the 0.5 eV wide stability region for  $\text{CuInSe}_2$  [54]. Based on ab initio calculations and experimental results, it is considered that single-phase kesterite is far more difficult to prepare compared to chalcopyrites.

So far, high-efficiency CZTS-based solar cells were found to have slightly Cu-poor and Zn-rich composition in general. It is observed that irrespective of the deposition technique or absorber preparation method, the best solar cells were obtained around a composition ratio of  $\sim 0.8-0.9$  for  $\text{Cu}/(\text{Zn} + \text{Sn})$  and  $\sim 1.1-1.2$  for  $\text{Zn}/\text{Sn}$ . From selected published literature data, an efficiency map is generated against the  $\text{Cu}/(\text{Zn} + \text{Sn})$  and  $\text{Zn}/\text{Sn}$  ratios as shown in Fig. 2.5a. Experimental data plotted in the ternary phase diagram as shown in Fig. 2.5b provides a clear idea of the confined composition space to realize high-efficiency CZTS-based solar cells. It is observed that the stoichiometric CZTS(Se) devices were limited to only  $\sim 5\%$  efficiency range, suggesting that Zn-rich composition is favorable.

During the absorber layer fabrication process, secondary phases such as  $\text{ZnS}(\text{Se})$  and  $\text{Cu}_2\text{SnS}(\text{Se})_3$  may form in the Zn-rich regime. Nagoya et al. [48] and Maeda et al. [55] have theoretically predicted  $\text{ZnS}$  to be the predominant impurity phase under the Cu-poor and Zn-rich growth condition with  $\text{Cu}_{\text{Zn}}$  antisite being the most stable defect in the entire stability region of CZTS [53].

Existence of the  $\text{ZnSe}$  secondary phase in  $\text{Cu}_2\text{ZnSnSe}_4$  films has been experimentally confirmed [56, 57].  $\text{ZnS}(\text{Se})$  has a wider bandgap and is usually less conductive and therefore is not considered to be responsible for reduced open-circuit voltage or reduced shunt resistance, but can lead to high series resistance of the solar cell [30, 56]. Other secondary phases such as  $\text{SnS}(\text{Se})_x$ ,  $\text{CuS}(\text{Se})_x$ , or Cu-Sn sulfide(selenide) are considered to be more detrimental because of their lower bandgap and high conductivity, which can significantly reduce the

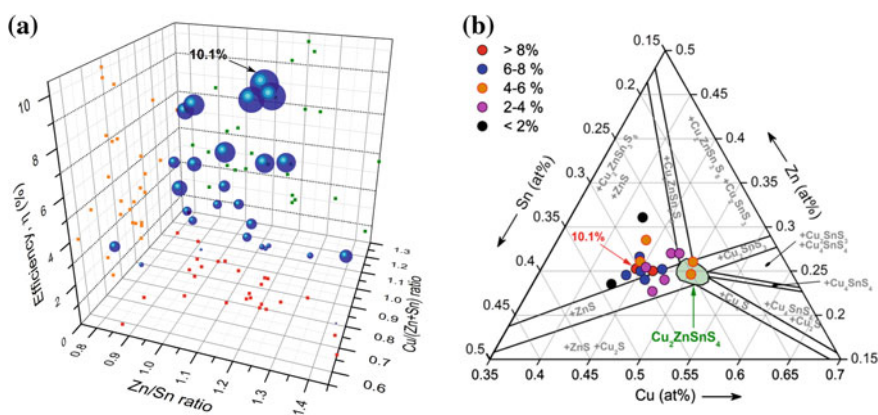


**Fig. 2.5** **a** Efficiency map for CZTS-based solar cells plotted against  $\text{Cu}/(\text{Zn} + \text{Sn})$  and  $\text{Zn}/\text{Sn}$  composition ratios and **b** solar cell efficiencies plotted in the ternary phase diagram

open-circuit voltage and decrease the shunt resistance leading to much inferior photovoltaic performance of the cell [42].

## 2.5 Etching

Surface preparation of semiconductors is important to achieve improved junction properties, reducing the recombination at the interface. For CZTS absorbers, KCN etching has been regularly performed to remove  $\text{Cu}_{2-x}\text{S}$  phases from the surface, improving the device performance. Influence of KCN etching on the chemical and electronic structure of CZTS films has been studied by Bär et al. [58]. It was observed that KCN preferentially etches Cu and some amount of Sn, changing the surface composition of CZTS films and widening the surface bandgap from 1.53 to 1.91 eV. However, air voids are often formed after the etching.

Katagiri et al. [59] have introduced a simple and non-hazardous etching process by soaking the absorber film in DI water. The CZTS/CdS heterojunction was fabricated after 10-min DI water soaking of the absorber, resulting in improved efficiency. The authors concluded that metal oxide particles on the absorber surface were removed in this process. Electron probe micro analysis (EPMA) showed that oxygen concentration on the film surface was significantly reduced as a result of the DI water soaking (Fig. 2.6).

Timmo et al. [60] studied the effect of different etching agents on  $\text{Cu}_2\text{ZnSn}(\text{S},\text{Se})_4$  monograins including HCl, KCN,  $\text{NH}_4\text{OH}$ , and Br-methanol. They observed that HCl could effectively etch Sn and Se, KCN has a preferential etching effect on Cu, Sn, and chalcogens, whereas  $\text{NH}_4\text{OH}$  preferentially etched copper and chalcogens. A tin-rich CZTS surface was obtained by Br-methanol etching.

Fairbrother et al. [61] showed that HCl etching drastically enhanced the device efficiency almost twofold compared to a device without any etching. The process was less hazardous and more effective than KCN etching. Experiments were carried out on CZTS films with Cu-poor and Zn-rich composition, which typically show

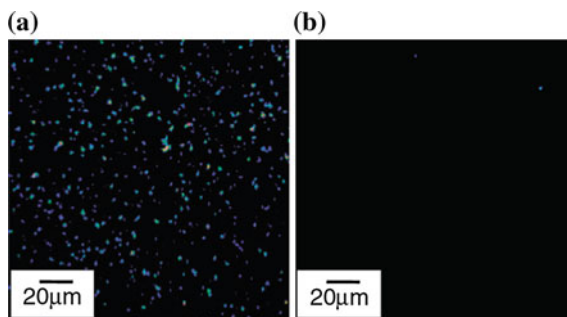


**Fig. 2.6** Oxygen distribution (*bright points*) on CZTS surface: **a** before DI water soaking and **b** after 4 h DI water soaking [59]

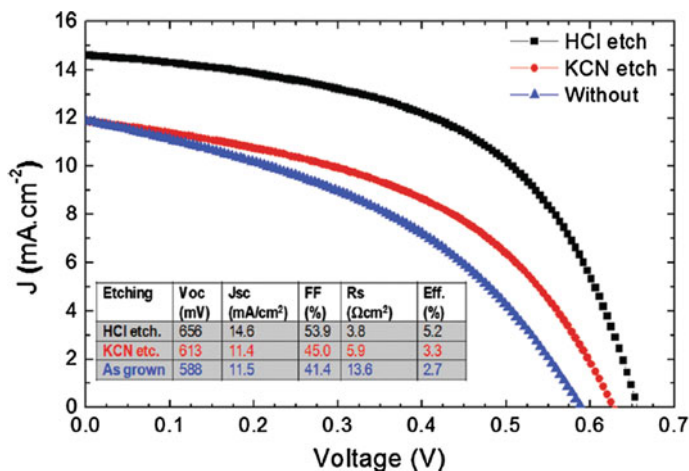


**Fig. 2.7**  $J$ - $V$  characteristics of the solar cells prepared using HCl-etched, KCN-etched, and without etched CZTS absorber layers [61]

superior photovoltaic performance. The authors suggested that HCl preferentially removes the Zn-rich secondary phases formed on the film surface leading to low series resistance, improved fill factor, and enhanced conversion efficiency. A device efficiency of 5.2 % was achieved with HCl etching compared to 3.3 and 2.7 % for KCN and unetched samples, respectively (Fig. 2.7).

## 2.6 Defects

Defects play an important role in the resulting optoelectronic properties of semiconductor materials. There are thirteen possible isolated intrinsic point defects in kesterite structure that may form during the CZTS(Se) thin film/bulk crystal growth including vacancies ( $V_{Cu}$ ,  $V_{Zn}$ ,  $V_{Sn}$ , and  $V_S$ ), antisites ( $Cu_{Zn}$ ,  $Zn_{Cu}$ ,  $Cu_{Sn}$ ,  $Sn_{Cu}$ ,  $Zn_{Sn}$ , and  $Sn_{Zn}$ ), and interstitial defects ( $Cu_i$ ,  $Zn_i$ , and  $Sn_i$ ). Existence of point defects and deviation from the ideal stoichiometry lead to the self-doping and intrinsic p-type conductivity of CZTS(Se).

Several theoretical defect studies based on density functional theory (DFT)/first-principle calculations have been employed to investigate the defect mechanism and formation energies of different possible point defects in kesterites [48, 49, 51, 53, 55, 62–64]. Chen and co-workers have thoroughly studied the defect characteristics of CZTS(Se) [38, 53, 65, 66]. The polyhedron for the stable region of CZTS and CZTSe in the ( $\mu_{Cu}-\mu_{Zn}-\mu_{Sn}$ ) three-dimensional space with  $\mu_{Cu} = -0.2$  eV is shown in Fig. 2.8 [65], and the calculated defect formation energies of various isolated point defects (vacancies, antisites, and interstitials) as a function of Fermi energy at the chemical potential point  $P$  of the polyhedron is



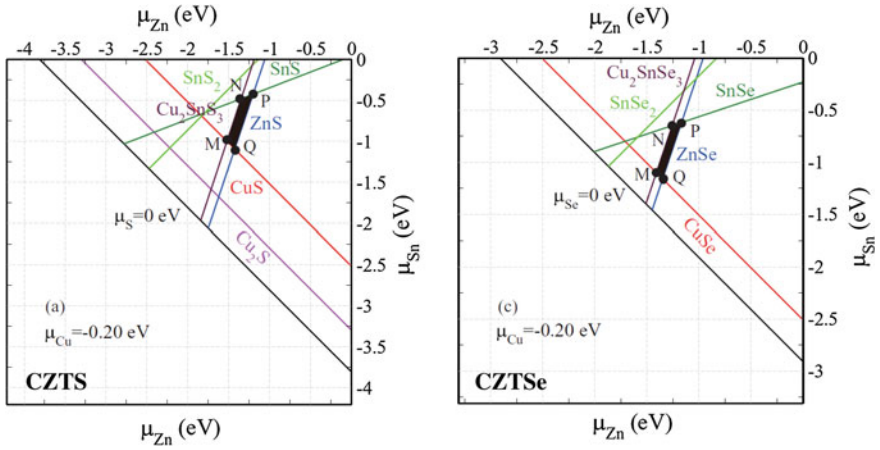


**Fig. 2.8** Stable chemical potential area (*black*) of  $\text{Cu}_2\text{ZnSnS}_4$  (CZTS) and  $\text{Cu}_2\text{ZnSnSe}_4$  (CZTSe) in  $(\mu_{\text{Zn}}, \mu_{\text{Sn}})$  planes with  $\mu_{\text{Cu}} = -0.20$  eV in  $(\mu_{\text{Cu}}, \mu_{\text{Zn}}, \mu_{\text{Sn}})$  three-dimensional chemical potential space [65]

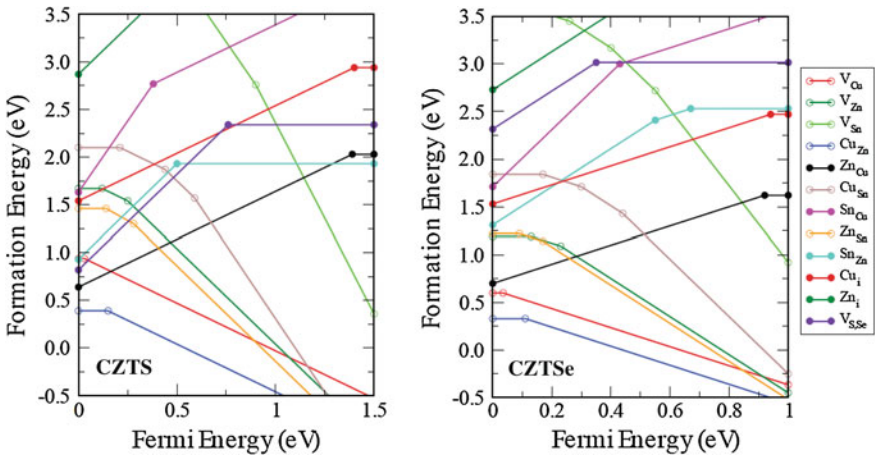


**Fig. 2.9** Change of defect formation energies in  $\text{Cu}_2\text{ZnSnS}_4$  (*left*) and  $\text{Cu}_2\text{ZnSnSe}_4$  (*right*) as a function of the Fermi energy at the chemical potential point *P* (see Fig. 2.8). For the same Fermi energy, only the most stable charge state is plotted, and the charge state changes at the *circles* (open for acceptors and filled for donors), which show the transition energy levels [65]

represented in Fig. 2.9. Out of the possible 13 point defects mentioned above, the lowest five formation energies in ascending order correspond to  $\text{Cu}_{\text{Zn}}$ ,  $\text{V}_{\text{Cu}}$ ,  $\text{Zn}_{\text{Sn}}$ ,  $\text{V}_{\text{Zn}}$ , and  $\text{Cu}_{\text{Sn}}$ , respectively, for Cu-poor kesterite as represented in Fig. 2.9.

All investigations converge to the general agreement that the acceptor defects such as  $\text{Cu}_{\text{Zn}}$  or  $\text{Cu}_{\text{Sn}}$  antisites and the Cu vacancy ( $\text{V}_{\text{Cu}}$ ) have lower energy of formation with the lowest formation energy for  $\text{Cu}_{\text{Zn}}$  antisite defect (Fig. 2.9). The

donor defects such as the S vacancy ( $V_S$ ) and the  $Zn_{Cu}$  antisite have much higher energy of formation. Such low formation energies of the acceptor defect levels, particularly  $Cu_{Zn}$  antisite, suggest the favorable formation of acceptors and are generally attributed to the evolution of p-type characteristics of  $Cu_2ZnSnS_4$  [67–75] and  $Cu_2ZnSnSe_4$  [76–79]. This explains why CZTS(Se) has always been reported to be of p-type regardless of the deposition method, and CZTS(Se) films for high-efficiency solar cells have shown Cu-poor and Zn-rich stoichiometry.

The  $Cu_{Zn}$  acceptor level is predicted to lie about 0.1 eV above the valence band maximum (VBM) compared to the shallower acceptor  $V_{Cu}$  at  $\sim 0.02$  eV above the VBM [53]. It is suggested that Cu vacancy ( $V_{Cu}$ ) is preferred than the  $Cu_{Zn}$  antisite for high-performance solar cells, since  $Cu_{Zn}$  antisite produces deeper acceptor level than that of the  $V_{Cu}$  [53]. The  $Cu_{Sn}$  antisite energy level lying near the mid-gap ( $\sim 0.6$  eV above the VBM) is predicted to be the most active deep recombination center for the charge carriers [53, 80].

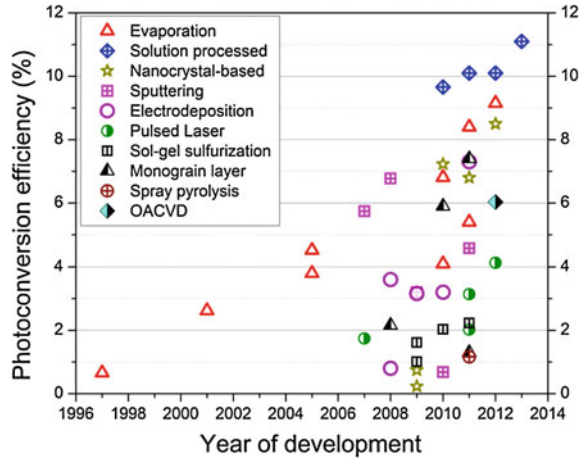
The  $Cu_{Zn}$  substitution occurs at the  $2d$  site, and  $Zn_{Cu}$  substitutions occur at the  $2c$  site [81, 82]. The existence of charge-compensated electrically neutral defect complexes such as  $[Cu_{Zn}^- + Zn_{Cu}^+]^0$  and  $[V_{Cu}^- + Zn_{Cu}^+]^0$  are also predicted for Cu-rich, Zn-poor and Cu-poor, Zn-rich CZTS, respectively [49]. However, such electrically benign defect pairs are believed to help in screening and electronic passivation of the deep levels, thus reducing the charge carrier recombination resulting in improved device performance [48, 53, 55].

In addition, two deep defect levels corresponding to activation energies of 0.12 and 0.167 eV have been experimentally identified via admittance spectroscopy of monograin CZTS solar cells which were attributed to  $Cu_{Zn}$  deep acceptor level and to interface states, respectively [83].

## 2.7 Deposition Techniques

Several physical and chemical deposition methods have been investigated for the fabrication of CZTS(Se) thin film absorber layer including thermal evaporation, electron beam evaporation, atom beam sputtering, RF/DC magnetron sputtering, hybrid sputtering, pulsed laser deposition (PLD), electrochemical deposition, solution-processed, nanoparticle-based synthesis, sol-gel spin coating, spray pyrolysis, chemical bath deposition (CBD), open-atmosphere chemical vapor deposition (OACVD), successive ion layer adsorption and reaction (SILAR), and screen printing. The main driving force for exploring different deposition methods is to develop a suitable absorber preparation technique to realize commercially viable low-cost and high-efficiency CZTS(Se) thin film solar cells. Such deposition techniques can be broadly classified as vacuum-based and non-vacuum deposition methods. The vacuum-based techniques are categorized as the methods requiring sophisticated instrumentation for deposition of precursor materials or absorber film fabrication under high vacuum. All physical vapor deposition (PVD) techniques—thermal evaporation, e-beam evaporation, atom beam sputtering, RF/DC magnetron

**Fig. 2.10** Evolution of CZTS (Se)-based solar cell efficiency using different deposition techniques



sputtering, hybrid sputtering, and pulsed laser deposition (PLD) fall into this category. On the other hand, the non-vacuum absorber deposition techniques promise high-throughput roll-to-roll production opportunity at reduced cost. Deposition techniques such as electrochemical deposition, solution processing, nanoparticle-based synthesis, sol-gel spin coating, spray pyrolysis, chemical bath deposition (CBD), open-atmosphere chemical vapor deposition (OACVD), successive ion layer adsorption and reaction (SILAR), and screen printing are classified as non-vacuum deposition methods.

Efficiency of the CZTS(Se)-based thin film solar cells has been improved significantly over the past decade since the first report by Katagiri et al. in 1997 [73]. The evolution of efficiency using different deposition techniques is illustrated in Fig. 2.10. All types of deposition methods have realized noticeable improvement over the years. Details of the deposition methods and corresponding solar cell device characteristics are summarized in Table 2.1.

So far, the best photovoltaic performance has been achieved by Se-enriched CZTS absorber layer (CZTSSe) deposited using a non-vacuum solution-processed technique developed by IBM. A solar cell efficiency of 11.1 % was reported for CZTSSe-based device [24]. Only sulfur-containing (Se free) CZTS solar cell has reached an efficiency of 8.4 %, and only Se-containing CZTSe solar cell has been reported with an efficiency of 9.15 %, respectively, employing vacuum-based evaporation technique [14, 84]. The efficiencies > 3 %, achieved by different vacuum and non-vacuum methods for CZTS, CZTSe, and CZTSSe absorbers, are depicted in Fig. 2.11.

### 2.7.1 Vacuum-Based Deposition Methods

Vacuum-based absorber layer fabrication techniques can be subclassified into one-step or two-step processes. Unlike CIGS, the vacuum-based CZTS(Se) absorber layer fabrication technique had been exclusively the two-step process. In a

**Table 2.1** Summary of various deposition methods Table of various deposition methods and device characteristics and their corresponding absorber composition and device characteristics taken from selected published literature

Deposition technique	$V_{oc}$ (mV)	$J_{sc}$ (mA/cm <sup>2</sup> )	Fill factor (FF)	Efficiency	Year	Compositional details		References		
						Absorber type	Cu/(Zn + Sn)		Zn/Sn	
Evaporation	400	6.0	27.7	0.66	1997	CZTS	–	[73]		
	522.4	14.11	35.54	2.62	2001	CZTS	–	[74]		
	661	19.5	65.8	8.4	2011	CZTS	–	[84]		
	629	12.53	58.0	4.53	2005	CZTS	–	[86]		
	436	6.0	41.0	1.1	2008	CZTS	–	[96]		
	587	17.8	65.0	6.81	2010	CZTS	0.82	1.2	[17]	
	377	37.4	64.9	9.15	2012	CZTSe	0.86	1.15	[14]	
	652	9.6	61.0	3.8	2005	CZTS	0.84	1.16	[151]	
	541	13.0	59.8	4.1	2010	CZTS	1.01	1.02	[87]	
	272	36.8	38.2	3.82	2011	CZTSe	0.59	0.86	[152]	
	497	20.0	–	–	2011	CZTSSe	0.78	0.97	[91]	
	478	9.78	38.0	1.79	2008	CZTS	0.96	1.18	[85]	
	422	29.5	60.0	7.51	2011	CZTSSe	–	–	[153]	
	247	26.84	43.5	2.88	2013	CZTSe	0.57	2.35	[154]	
	Sputtering	610	17.9	62.0	6.77	2008	CZTS	0.85	1.25	[59]
		662	15.7	55.0	5.74	2007	CZTS	–	–	[109]
		545	15.44	54.6	4.59	2011	CZTS	0.67	1.45	[99]
359		20.7	43.0	3.2	2009	CZTSe	0.83	1.15	[100]	
523		15.1	38.0	3.01	2011	CZTS	0.89	0.96	[101]	
718		10.9	41.0	3.2	2011	CZTS	0.92	0.93	[155]	
345		4.42	44.3	0.68	2010	CZTS	–	–	[102]	
620		11.8	63.0	4.5	2012	CZTS	–	–	[156]	
462		22.8	62.1	6.6	2012	CZTSSe	0.73	1.1	[157]	

(continued)

Table 2.1 (continued)

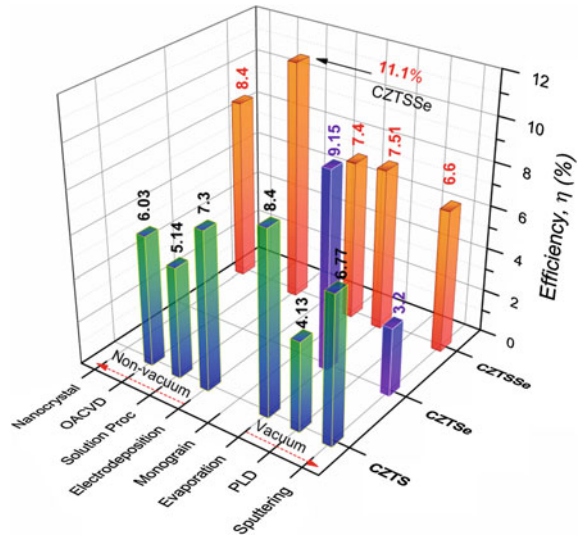
Deposition technique	$V_{oc}$ (mV)	$J_{sc}$ (mA/cm <sup>2</sup> )	Fill factor (FF)	Efficiency	Year	Compositional details			References
						Absorber type	Cu/(Zn + Sn)	Zn/Sn	
Pulsed laser deposition (PLD)	651	8.76	55.0	3.14	2011	CZTS	–	–	[116]
	546	6.78	48.4	1.74	2007	CZTS	0.73	0.86	[112]
	585	6.74	51.0	2.02	2011	CZTS	–	–	[117]
	700	10.01	59.0	4.13	2012	CZTS	–	–	[118]
Solution processing	517	30.8	63.7	10.1	2011	CZTSSe	–	–	[135]
	516	28.6	65.0	9.66	2010	CZTSSe	0.8	1.22	[134]
	422.8	38.7	61.9	10.1	2012	CZTSSe	0.8	1.2	[15]
	516.9	18.9	52.8	5.14	2012	CZTS	0.99	0.93	[158]
	459.8	34.5	69.8	11.1	2013	CZTSSe	–	–	[24]
	400	24.9	41.2	4.1	2011	CZTSSe	0.8	1.13	[159]
	430	31.2	53.9	7.23	2010	CZTSSe	0.79	1.1	[18]
Nanocrystal-based synthesis	321	1.95	37.0	0.23	2009	CZTS	–	–	[123]
	451	29.0	64.9	8.5	2012	CZTSSe	–	–	[126]
	640	21.5	49.0	6.8	2011	CZTGeS	–	–	[160]
	529	10.2	41.6	2.23	2011	CZTS	0.9	1.32	[161]
Sol-gel sulfuration	575	9.69	36.4	2.03	2010	CZTS	0.92	1.17	[162]
	554	6.7	43.4	1.61	2009	CZTS	0.96	1.17	[163]
	390	7.8	33.0	1.01	2009	CZTS	–	–	[164]
	358	5.06	34.7	0.63	2011	CZTS	0.75	1.43	[165]
	381	15.8	42.1	2.76	2012	CZTSe	0.79	1.39	[166]
	582.4	7.13	32.0	1.3	2011	CZTS	–	–	[83]
	622	15.87	60.0	5.9	2010	CZTSSe	–	–	[148]
Monograin layer (MGL)	422	15.5	44.0	2.16	2008	CZTSe	–	–	[149]
	720	18.4	60.0	7.4	2011	CZTSSe	0.89	1.1	[150]

(continued)

**Table 2.1** (continued)

Deposition technique	$V_{OC}$ (mV)	$J_{SC}$ (mA/cm <sup>2</sup> )	Fill factor (FF)	Efficiency	Year	Compositional details			References
						Absorber type	Cu/(Zn + Sn)	Zn/Sn	
Electrodeposition	567	22.0	58.1	7.3	2011				[138]
	529	15.9	42	3.6	2009	CZTS	0.97	1.08	[139]
	540	12.6	46.4	3.16	2009	CZTS	–	–	[140]
	540	16.9	40	3.6	2013	CZTSSe	–	–	[145]
Screen printing	386	4.76	27.0	0.49	2010	CZTS	–	–	[167]
	250	8.76	27.0	0.6	2012	CZTS	–	–	[168]
Spray pyrolysis	410	8.0	35.5	1.16	2011	CZTS	–	–	[169]
	175	0.46	24.5	0.154	2012	CZTS	–	–	[170]
OACVD	658	16.5	55.0	6.03	2012	CZTS	0.78	1.29	[136]
Chemical bath deposition	210	2.4	–	0.16	2010	CZTS	–	–	[171]
SILAR	280.5	0.637	62.0	0.396	2012	CZTS	–	–	[104]

**Fig. 2.11** Best photoconversion efficiencies achieved via different vacuum and non-vacuum deposition techniques using pure CZTS, pure CZTSe, and mixed CZTSSe solar absorber layers



two-step process, the first step involves the deposition of constituent elements of CZTS(Se) compound onto a substrate by deposition of pure elemental metals (Cu/Zn/Sn) or a combination of elemental and binary chalcogenides (such as Cu/ZnS/SnS). They can be either deposited in a stacked layer fashion or co-deposited together to achieve the desired composition in the final film. In the second step, the CZTS(Se) film growth and incorporation of balance chalcogen atoms (S/Se) are achieved by an atmospheric thermal processing of the substrate under S/Se vapor or  $\text{H}_2\text{S}(\text{Se})$  gas flow. Recently, a one-step absorber layer fabrication process had been reported for CZTSe solar cell, where the deposition and film growth were achieved in a single step by controlled evaporation of all constituent elements (Cu, Zn, Sn, and Se) inside the vacuum chamber under elevated substrate temperature yielding 9.15 % champion cell [14]. The one-step process can be considered superior compared to the two-step process from commercial point of view, as it eliminates the hazardous thermal processing step, reducing the time and cost of fabrication. This section will review the various vacuum-based deposition techniques employed to prepare CZTS(Se) solar cells and the notable results reported in the literature.

### 2.7.1.1 Evaporation

Evaporation is a well-established technique for the fabrication and development of thin film solar cells. Various types of evaporation technologies such as electron beam evaporation, thermal evaporation including co-evaporation, and fast evaporation have been investigated to fabricate CZTS(Se) absorber layer [14, 17, 73, 74, 84–97].

In 1997, the first photovoltaic performance of a CZTS-based thin film solar cell was reported by Katagiri et al. with an open-circuit voltage ( $V_{OC}$ ) of 400 mV, short-circuit current density ( $J_{SC}$ ) of 6 mA/cm<sup>2</sup>, and a photoconversion efficiency of 0.66 % [73]. The absorber layer was fabricated by sequential deposition of Zn/Sn/Cu elemental stacked precursor layers on Mo-coated soda-lime glass (SLG) substrate by electron beam evaporation at 150 °C substrate temperature followed by sulfurization of the precursor layers under N<sub>2</sub> + H<sub>2</sub>S (5 %) flow at 500 °C for 1–3 h. The heterojunction was formed by the deposition of n-CdS window layer on the p-type CZTS film. Since then, evaporation technique has been intensively used in the development of CZTS (Se) solar cells.

The same year, Friedlmeier et al. [88] reported CZTS solar cell with 2.3 % efficiency, fabricated by thermal evaporation of elemental metals and binary chalcogenides under high vacuum. Later, in 2001, Katagiri et al. [74] further improved the efficiency by replacing the elemental Zn with ZnS in the precursor layer and subsequent sulfurization at an increased temperature of 550 °C under H<sub>2</sub>S flow for 1 h. The substrate temperature was also elevated up to 400 °C during the precursor layer deposition. Absorbers with different thicknesses from 0.95 to 1.63 μm were fabricated to study the effect on the photovoltaic response of the resulting devices. XRD peaks corresponding to (112), (200), (220/204), and (312/116) planes with a preferential orientation along [112] were observed and attributed to the kesterite structure. Film compositions were found slightly Cu-poor and Zn-rich with an optical absorption coefficient >10<sup>4</sup> cm<sup>-1</sup> and a bandgap of 1.45 eV for the best performing cell. A significant decrease of the short-circuit current density and fill factor were observed with increasing thickness of the CZTS active layer, leading to drastically reduced efficiency. The best solar cell with Al/ZnO:Al/CdS/CZTS/Mo-SLG device configuration showed a photoconversion efficiency of 2.62 % [74]. By optimization of the sulfurization process and the device structure, the same group of researchers developed a device with 5.45 % efficiency in 2003 with a reported  $V_{OC}$  = 582 mV,  $J_{SC}$  = 15.5 mA/cm<sup>2</sup>, and 60 % fill factor [89].

Large dependence of Cu/(In + Ga) ratio on the optoelectronic properties of CIGS thin film motivated the investigation of such dependence in CZTS solar cells by varying the Cu/(Zn + Sn) ratio [98]. Kobayashi et al. [86] studied the effect of Cu/(Zn + Sn) and the sulfurization temperature on the resulting film properties prepared via e-beam evaporation. CZTS absorbers were prepared with the varying Cu/(Zn + Sn) ratio ranging from 0.49 to 1.18 in the final film, and the sulfurization temperature was varied from 510 to 550 °C. The best photovoltaic performance was obtained for the CZTS film sulfurized at 520 °C with measured elemental ratios of Cu/(Zn + Sn) = 0.85, Zn/Sn = 1.03, and S/metal = 1.18. The best solar cell exhibited an efficiency of 4.53 % with  $V_{OC}$  = 629 mV,  $J_{SC}$  = 12.53 mA/cm<sup>2</sup>, and FF = 58 %. Araki et al. [85] studied the influence of different stacking orders of elemental Zn, Sn, and Cu in the precursor layer on the film properties. Stacked precursor layers with six possible sequences were fabricated by e-beam evaporation on Mo-coated borosilicate glass and subsequently sulfurized at 560 °C for 2 h under the flow of elemental sulfur vapor to form CZTS films. Surface morphology,



composition, and electronic properties of the resulting films were found to be highly dependent on the precursor layer stacking order. The best cell was obtained for the precursor with a Mo/Zn/Cu/Sn stacking configuration yielding a photoconversion efficiency of 1.79 %. It was observed that considerably higher efficiency is achieved for the films with Cu and Sn layers placed adjacent to each other.

Wang et al. developed a simple two-step method where film processing time was significantly reduced to few minutes compared to the previous reports of  $\text{H}_2\text{S}$  processing requiring hours of annealing. They prepared high-quality PV-grade CZTS films by thermal co-evaporation of constituent elements on Mo/SLG substrates held at  $110^\circ\text{C}$  followed by a hot-plate annealing for 5 min at  $540^\circ\text{C}$  under sulfur vapor [17]. Absorber layers with different thicknesses ranging from 0.65 to  $1.2\ \mu\text{m}$  were fabricated. Raman spectra showed the CZTS characteristic peaks corresponding to 287, 338, and  $368\ \text{cm}^{-1}$  without the presence of any secondary phases. Similar to the observation made by Katagiri et al. [74], a significant reduction in efficiency was observed with increasing absorber thickness mainly due to degraded fill factor. The completed device had a configuration of SLG/700 nm Mo/CZTS absorber/70 nm CdS/80 nm i-ZnO/460 nm Al:ZnO or 180 nm ITO/Ni-Al metal fingers. A  $105\ \text{nm}\ \text{MgF}_2$  antireflection coating was applied on top of the cell. The champion device (device D in Fig. 2.12a) showed a photoconversion efficiency of 6.8 % ( $V_{\text{OC}} = 587\ \text{mV}$ ,  $J_{\text{SC}} = 17.8\ \text{mA}/\text{cm}^2$ , and  $\text{FF} = 65\%$ ) with an absorber layer thickness of  $0.65\ \mu\text{m}$ . The  $J$ - $V$  characteristics of the cells with different absorber layer thickness are presented in Fig. 2.12a.

The device performance was limited by high series resistance ( $R_s$ ). A strong temperature dependence of  $R_s$  indicated the existence of a back-contact blocking layer (Schottky barrier) at the Mo/CZTS interface, suppressing the hole transport from the absorber to the Mo back contact. A barrier height of 0.32 eV for the blocking back contact was estimated from temperature-dependent measurement of the series resistance, and an activation energy of 1.05 eV corresponding to the

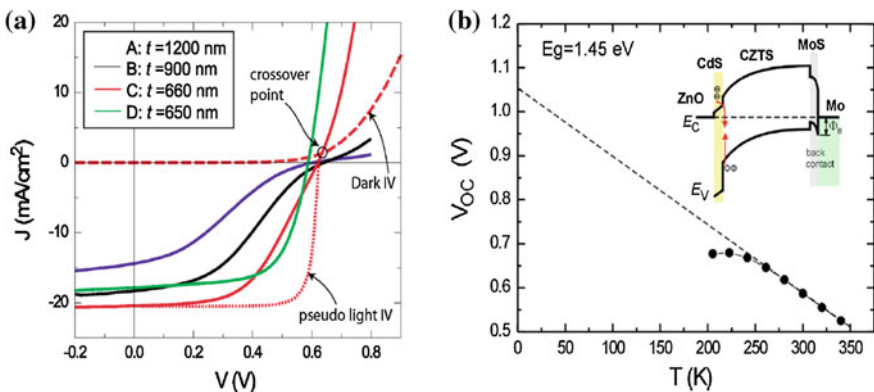


**Fig. 2.12** **a**  $J$ - $V$  curves of solar cells with different CZTS absorber thickness. The dark  $J$ - $V$  and the pseudo  $J$ - $V$  correspond to device C, **b** open-circuit voltage ( $V_{\text{OC}}$ ) versus temperature plot of device C. A hypothetical band diagram showing the dominant recombination pathway at the CdS buffer/CZTS absorber interface and presence of a blocking back contact [17]

dominant recombination loss was extracted from the temperature-dependent  $V_{OC}$  measurement. A hypothetical band diagram was proposed based on these measurements, and the authors suggested that the subbandgap activation energy corresponds to the interfacial recombination at the CdS/CZTS interface, leading to lower open-circuit voltage (Fig. 2.12b).

Following the same procedure developed by Wang et al. [17], an 8.4 % efficient CZTS solar cell was reported by Shin et al. [84]. CZTS films were fabricated by thermal co-evaporation of constituent elements and 5 min atmospheric annealing at 570 °C. The device structure was as follows: Mo-coated SLG/ ~600 nm CZTS/90–100 nm CdS/80 nm i-ZnO/450 nm Al:ZnO/Ni–Al metal fingers/100 nm MgF<sub>2</sub>. A bimodal grain size distribution was observed with larger grains comparable to the film thickness in the bulk of the film and much smaller grains at the immediate vicinity of the Mo back contact (Fig. 2.13a). The EDX line scan data perpendicular to the substrate (shown by the red arrow in Fig. 2.13a) revealed that the smaller grains correspond to an interfacial ZnS layer near the Mo back contact, whereas the larger grains in the bulk of the film are CZTS compound (Fig. 2.13b).

A depletion layer width of 180 nm and minority carrier diffusion length larger than 350 nm was estimated from time-resolved photoluminescence (TRPL) measurements and drive-level capacitance measurements. The champion cell exhibited  $V_{OC} = 661$  mV,  $J_{SC} = 19.5$  mA/cm<sup>2</sup>, and a fill factor of 65.8 % (Fig. 2.14).

Loss of Sn under high vacuum during the annealing process for the Cu–Zn–Sn–S, Cu–Sn–S, and Sn–S material systems was investigated by Weber et al. [90]. Experimental results showed that Sn loss occurs in these systems as volatile SnS above 350 °C at a pressure of  $1 \times 10^{-2}$  Pa and the rate of Sn loss is increased significantly at temperatures above 550 °C. Decomposition of ternary Cu<sub>2</sub>SnS<sub>3</sub> and Cu<sub>4</sub>SnS<sub>4</sub> and quaternary Cu<sub>2</sub>ZnSnS<sub>4</sub> phases leaves Cu<sub>x</sub>S and ZnS solid phases in the annealed films. They suggested the decomposition reaction to take place following the reaction paths as summarized in (2.1)–(2.3). The authors suggested CZTS film processing at temperatures less than 550 °C under an inert gas ambient to minimize high degree of Sn loss and decomposition of CZTS.

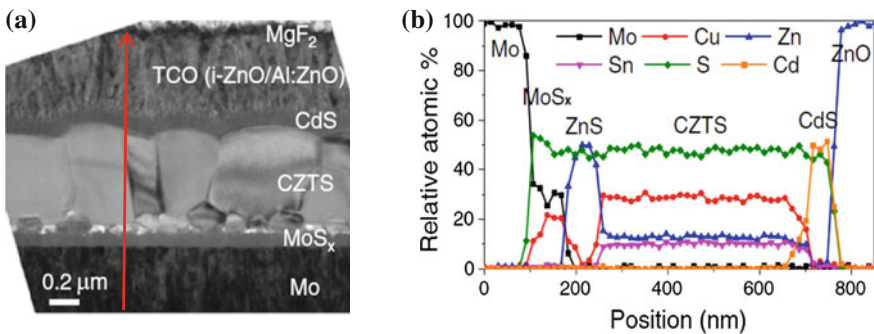
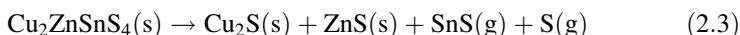
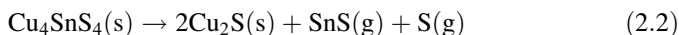
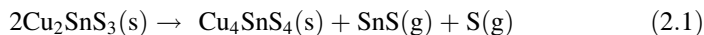
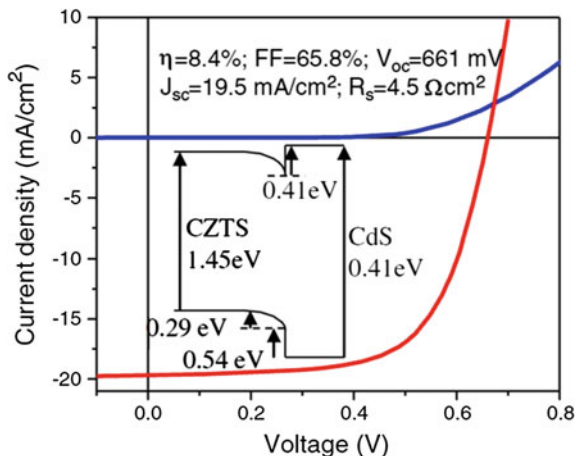


**Fig. 2.13** **a** Bright-field cross-sectional TEM image of the champion CZTS device (Se free) and **b** EDX line scan along the red arrow in Fig. 2.13a showing the elemental profile [84]

**Fig. 2.14**  $J$ - $V$  characteristics of the solar cell with 8.4 % efficiency *under dark* and under 1 sun illumination. Band alignment of CdS buffer with the CZTS absorber layer is depicted in the *inset* [84]



Redinger et al. addressed this issue by introducing extra Sn along with excess sulfur during the annealing process [91]. They prepared the CZTSe films by co-evaporation of Cu, Zn, Sn, and Se under high vacuum followed by annealing at 560 °C for 2 h under elemental S vapor. A dramatic increase of the device efficiency from 0.02 to 5.4 % was achieved with the addition of Sn in the annealing chamber. It was suggested that Sn in the presence of excess sulfur forms SnS during high-temperature processing of CZTS films and the partial pressure of volatile SnS creates a dynamic equilibrium with its solid-state counterpart in the film, resulting in suppression of Sn loss in the form of SnS from the CZTS precursor layer. The authors modified the proposed decomposition reaction path suggested by Weber et al. [90] to a reversible reaction mechanism under the improved annealing conditions in the presence of excess Sn.

In 2006, Tanaka et al. [92] reported on the growth of CZTS film by co-evaporation of elemental Cu, Zn, Sn, and sulfur simultaneously deposited for 3 h on quartz substrates held at 400–600 °C. Notably, this was the first report on the one-step film fabrication approach, although no photovoltaic performance was investigated. All films showed p-type conductivity with a strong preferred orientation along [112] plane. The grain sizes increased with increasing substrate temperature, and large columnar grains were reported to form at 550 °C. Later, in 2008, Oishi et al. adopted the similar approach to grow CZTS thin films on (110) Si wafers by one-step co-evaporation technique [93]. Films were fabricated by simultaneous deposition of Cu, ZnS, Sn, and sulfur for 3 h at substrate temperatures

from 430 to 500 °C. All films showed slightly Cu-rich and highly Zn-rich stoichiometry. XRD pattern revealed that the (112) peak intensity is decreased and (004)/(200) peak intensity is increased for the films grown at elevated temperature, suggesting a temperature-induced orientational growth at higher temperatures. Tanaka et al. [94] studied the influence of Cu/(Zn + Sn) on the physical properties of CZTS thin films prepared by one-step co-evaporation technique. CZTS films were grown by multisource evaporation of the constituent elements at 550 °C substrate temperature for 2 h. Cu/(Zn + Sn) ratio was varied from 0.82 to 1.06 keeping the constant Zn/Sn ratio at 1.1, and in a second set, Cu/(Zn + Sn) was varied from 0.82 to 1.28 with a constant Zn/Sn ratio of 0.95, while S/metal ratio was kept constant at 0.93 for all films. Structural, morphological, and electrical characteristics of the films were correlated with the film compositions. For Zn-rich films, the resistivities of the films were found to be highly dependent on the Cu/(Zn + Sn) ratio, but Sn-rich films did not show such dependency. An increase of the (112) peak intensity and a narrower FWHM in the X-ray diffraction pattern with increasing Cu/(Zn + Sn) ratio suggested an improved crystallinity which was supported by the larger grains evidenced in SEM micrographs. This important observation suggested that growth of high-quality larger grain CZTS film can be promoted by a Cu-rich growth condition similar to the benchmark CIGS films obtained by multistage evaporation, where the deposition process begins with Cu-rich condition and is controlled to terminate with a Cu-poor stoichiometry.

A fast (16 min) co-evaporation technique was introduced by Schubert et al. to fabricate CZTS absorber in one-step process [87]. Cu, ZnS, Sn, and sulfur were co-evaporated on Mo-coated SLG substrates held at 550 °C under constant sulfur partial pressure of  $2\text{--}3 \times 10^{-3}$  Pa. Due to the formation of a secondary CuS phase as evidenced from X-ray diffraction pattern, the as-grown films were highly Cu-rich with a Cu/(Zn + Sn) ratio of 1.42. The absorber layer was etched with aqueous KCN solution before CdS deposition to remove the excess CuS. As a result of KCN etching, the Cu/(Zn + Sn) ratio decreased to 1.01, resulting in nearly stoichiometric films. The best cell with a SLG/Mo/CZTS/CdS/Al:ZnO/Ni/Al device configuration showed a total area efficiency of 4.1 % with  $V_{OC} = 541$  mV,  $J_{SC} = 13.0$  mA/cm<sup>2</sup>, and FF = 59.8 %. So far, this holds the record for the high-efficiency CZTS solar cell produced via one-step vacuum co-evaporation technique.

Repins et al. [14] fabricated Cu<sub>2</sub>ZnSnSe<sub>4</sub> (CZTSe) solar cell with 9.15 % efficiency by co-evaporation. The CZTSe absorber layer was grown by four-source (Cu, Zn, Sn, and Se) thermal co-evaporation. A 15 nm NaF layer was deposited on Mo-coated SLG substrate by e-beam evaporation before the CZTSe film fabrication. The NaF layer was used to compensate the low out-diffusion of sodium. It was argued that the NaF deposition helped to improve the  $V_{OC}$ ,  $J_{SC}$ , and the fill factor. Deposition flux of each source and the substrate temperature were precisely controlled during the film growth (Fig. 2.15a). A Cu-rich growth was carried out for initial 12.5 min to favor larger grain growth, and the Cu source was turned off thereafter. Formation of Cu<sub>x</sub>Se<sub>y</sub> is expected during this period which further reacts with continuing Zn and Sn flux to form kesterite CZTSe film.

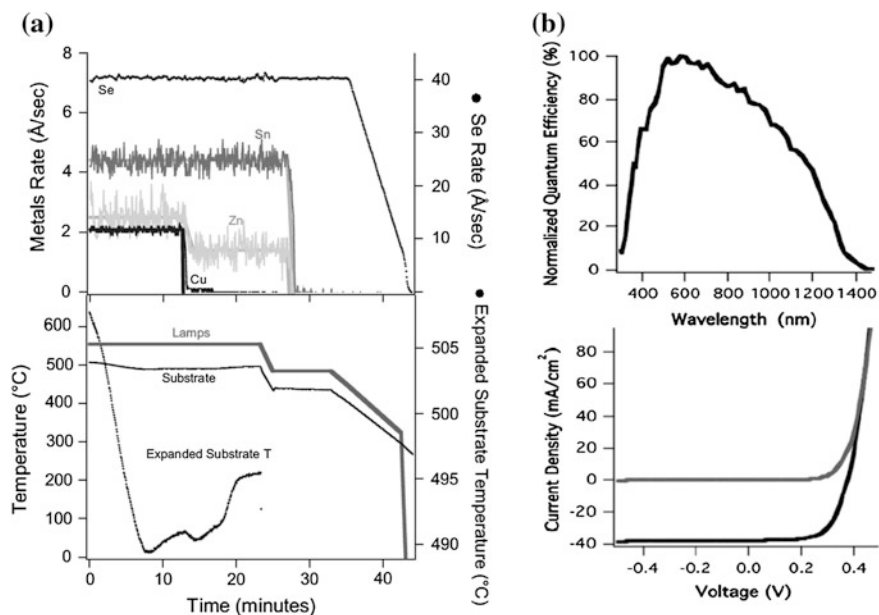


**Fig. 2.15** **a** Deposition rate of source materials (*top*) and substrate temperature profile (*bottom*); **b** external quantum efficiency (*top*) and the illuminated  $J$ - $V$  characteristic of the CZTSSe device with 9.15 % efficiency (*bottom*) [14]

The film composition was slightly Zn-rich and Cu-poor and was found to be uniform throughout the bulk with a Cu-poor surface. Void-free, large 0.5–1.0- $\mu\text{m}$  columnar grains with faceted surfaces extending the entire absorber thickness were observed. Single-phase kesterite CZTSSe without any secondary phases were detected by XRD and Raman measurements. The best solar cell with  $\sim 0.42 \text{ cm}^2$  total area exhibited  $V_{\text{OC}} = 377 \text{ mV}$ ,  $J_{\text{SC}} = 37.4 \text{ mA/cm}^2$ , and  $\text{FF} = 64.9 \%$ , yielding an efficiency of 9.15 % (Fig. 2.15b).

A high diode ideality factor of 1.8 and lower  $V_{\text{OC}}$  indicated dominant recombination in the device which was further confirmed by small carrier lifetime of 1–2 ns calculated from TRPL measurements. Notably, unlike the high-efficiency CZTS device reported by Wang et al. [17], no evidence of a blocking back contact was observed for the solar cells obtained in this process. Therefore, it can be concluded that formation of such blocking barrier is dependent on the particular deposition process and not an intrinsic issue related to the kesterite material system.

Controlling the deposition parameters play key role to obtain single-phase kesterite compound. Even a small presence of secondary phases could be highly detrimental to the resulting photovoltaic performance and by choosing the right deposition parameters, the undesired secondary Sn chalcogenides can be avoided in the resulting film [95]. XRD data showed that binary Sn chalcogenides can easily form at lower deposition temperature or if the Sn flux is continued below 450 °C during cooling down of the substrate. Similarly, control of Cu flux and Zn flux is

also important to obtain the absorber layer without binary Cu/Zn chalcogenides which can severely limit the solar cell performance.

A multistage evaporation technique was experimented by Weber et al. [96] to fabricate CZTS thin film absorber. Two different batches of samples were produced. In the first one, Cu–Sn–S (CTS) precursor was reacted with ZnS, and in the second one, ZnS precursor was reacted with Cu–Sn–S phase to promote CZTS growth. Both types of samples showed kesterite-type structure. Densely packed larger grains were observed for the second sample, and the highest efficiency of 1.1 % ( $V_{OC} = 436$  mV,  $J_{SC} = 6.0$  mA/cm<sup>2</sup>, and FF = 41 %) was achieved for this batch compared to the 0.7 % efficiency ( $V_{OC} = 501$  mV,  $J_{SC} = 4.2$  mA/cm<sup>2</sup>, and FF = 35 %) obtained from the first batch of samples with CTS precursor.

### 2.7.1.2 Sputtering

Sputtering is another well-established high-vacuum deposition technique widely used in the semiconductor industry to fabricate high-quality thin film devices. Different variations of sputtering technologies have been investigated to prepare CZTS(Se) thin film absorber materials including argon beam sputtering, DC/RF magnetron sputtering, and hybrid and reactive sputtering [68, 71, 99–108]. Similar to evaporation, CZTS(Se) film fabrication approach by sputtering techniques also could be subclassified into one-step or two-step processes.

Historically, the first report on the preparation and characterization of CZTS thin films made by Ito and Nakazawa in 1988 [71] employed sputtering technique. The absorber layer was deposited on Corning 7059 glass substrates at different temperatures by atom beam sputtering of quaternary target material synthesized by heating elemental powders to 1050 °C in a vacuum-sealed quartz ampoule. The deposited polycrystalline films showed a strong diffraction peak from (112) plane at substrate temperature higher than 90 °C, and the authors have suggested the crystal structure to be stannite type. An increase of the grain sizes and decrease of resistivity were observed for the films deposited at higher substrate temperatures due to the higher mobility of sputtered particles. A direct bandgap of 1.45 eV was measured for the film deposited at substrate temperature of 120 °C, and the absorption coefficient was in the range of 10<sup>4</sup> cm<sup>-1</sup>. Photovoltaic cells were fabricated on CZTS films deposited on stainless steel substrate at 160 °C. The heterodiode formed by the deposition of cadmium tin oxide window layer on CZTS absorber showed an open-circuit voltage of 165 mV. Shortly after, they improved the  $V_{OC}$  to 265 mV with a short-circuit current density of 0.1 mA/cm<sup>2</sup> by atmospheric annealing of the deposited film [103].

In 2003, Seol et al. [105] reported on CZTS thin films prepared by RF magnetron sputtering at room temperature using a cold-pressed target made of Cu<sub>2</sub>S, ZnS, and SnS<sub>2</sub> powders. The as-deposited films were sulfur-deficient and were subsequently annealed under Ar + S(g) atmosphere at 250–400 °C for 2 h to improve the S content. The ratio of Cu<sub>2</sub>S, ZnS, and SnS<sub>2</sub> was kept at 2:1.5:1 and the RF power between 50 and 100 W to obtain a stoichiometric CZTS film after

sulfurization. The films became Sn-rich and Cu-deficient as the RF power was increased over 100 W. XRD results showed strong diffraction peaks corresponding to (112), (200), (220), and (312) planes with a preferential orientation along (112) and showed improved crystallinity at higher annealing temperatures. The crystal structure was identified as kesterite type and the measured bandgap was 1.51 eV with an optical absorption coefficient of  $1 \times 10^4 \text{ cm}^{-1}$ .

Tanaka et al. [68] experimented with a hybrid sputtering system equipped with Cu and Sn sputtering sources and Zn and S effusion cells inside a high-vacuum chamber to achieve sequential deposition of Cu/Zn/Sn precursor layer followed by annealing under incident S flux to prepare CZTS films. Sn layer was deposited by DC sputtering, Zn layer by evaporation, and Cu layer was deposited by RF sputtering at different substrate temperatures from 300 to 500 °C. A decrease in film thickness was observed at higher substrate temperatures, which was attributed to reduced sticking coefficient and/or increased density due to improved crystallization. At lower substrate temperature (<350 °C), binary  $\text{Cu}_x\text{S}$  compounds were formed as identified from XRD analysis. Formation of stannite CZTS compound along with binary Cu sulfides started above 350 °C as evidenced by the evolution of CZTS (112) peak in the diffraction pattern. At 400 °C, single-phase stoichiometric CZTS film was obtained without the presence of any significant secondary phases. Above 450 °C, films were Zn-poor due to high vapor pressure of Zn, resulting in substantial Zn loss. Replacing Zn by ZnS or by introducing S flux during Zn deposition to form zinc sulfide was suggested to mitigate the Zn loss at higher substrate temperatures. The film obtained at 400 °C showed a direct bandgap of 1.5 eV with an optical absorption coefficient  $>10^4 \text{ cm}^{-1}$ . The films exhibited p-type conductivity with a carrier concentration of  $8 \times 10^{18} \text{ cm}^{-3}$ .

In order to avoid the effect of moisture adsorption from atmosphere during the film fabrication process, Jimbo et al. [109] developed an inline-type vacuum apparatus consisting of two interconnected chambers: one for precursor deposition by RF co-sputtering and the other for sulfurization of the precursor. Cu, ZnS, and SnS targets were co-sputtered to deposit the precursor film. After the precursor layer fabrication, the substrate was transferred to the annealing chamber without breaking the vacuum. Annealing was performed under  $\text{N}_2 + \text{H}_2\text{S}$  (20 %) environment at 580 °C for 3 h. The best solar cell showed  $V_{\text{OC}} = 662 \text{ mV}$ ,  $I_{\text{SC}} = 15.7 \text{ mA/cm}^2$ , and a fill factor of 55 %, leading to 5.74 % conversion efficiency. The composition of the CZTS absorber was found to be slightly Cu-deficient and Zn-rich with compositional ratios of  $\text{Cu}/(\text{Zn} + \text{Sn}) = 0.87$  and  $\text{Zn}/\text{Sn} = 1.15$ , respectively. An external quantum efficiency of 65 % at  $\lambda = 480 \text{ nm}$  and bandgap of 1.45 eV were measured.

Later in 2008, the same group of researchers further improved the efficiency by soaking the CZTS absorber in DI water prior to CdS window layer deposition [59].

The metal oxide particles in the film were removed by DI water, resulting in an improved device performance. The stoichiometry of the films was found to be Cu-poor and Zn-rich with elemental composition ratios of  $\text{Cu}/(\text{Zn} + \text{Sn}) = 0.85$ ,  $\text{Zn}/\text{Sn} = 1.25$ , and  $\text{S}/\text{metal} = 1.1$ , respectively. The champion cell showed an open-circuit voltage of 610 mV, short-circuit current density of  $17.9 \text{ mA/cm}^2$ , and a fill factor of 62 %, leading to an efficiency of 6.77 % after light soaking for 5 min

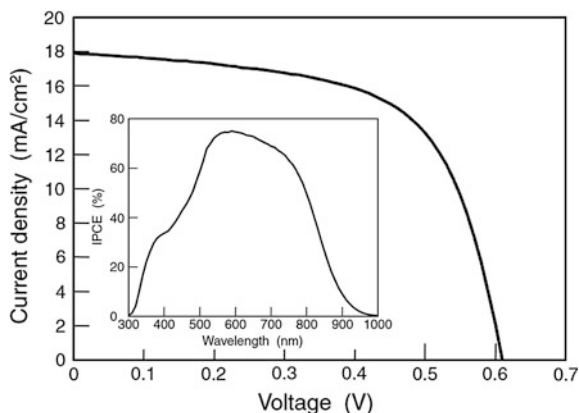
under AM 1.5 illumination. This is the highest efficiency cell fabricated by sputtering technique till date. An incident photon to current efficiency (IPCE) of  $>70\%$  was observed at  $\sim 550\text{ nm}$ . The  $J$ - $V$  characteristic and the IPCE curve showing the photovoltaic response of the device in the visible spectrum are shown in Fig. 2.16.

Similar to the study of Araki et al. [85], the effect of precursor layers' stacking order on the physical properties of resulting CZTS thin films was investigated by Fernandes et al. [104]. CZTS films were prepared with Mo/Zn/Cu/Sn and Mo/Zn/Sn/Cu initial metallic precursor stacking orders deposited by DC magnetron sputtering. Sulfurization of the precursor layer was performed in  $\text{N}_2 + \text{S}(\text{g})$  atmosphere at  $525\text{ }^\circ\text{C}$  for 10 min. However, contrary to the results obtained by Araki et al., the authors concluded the best precursor order to be Mo/Zn/Sn/Cu. It was argued that top Cu layer helped to reduce the Zn and Sn loss during the annealing process, leading to a better composition. Binary  $\text{Cu}_x\text{S}$  was detected on the film surface which was subsequently removed by KCN etching. The resulting films had a kesterite structure as confirmed by Raman spectroscopy. A sharp absorption edge at  $1.43\text{ eV}$  and a carrier concentration of  $3.3 \times 10^{18}\text{ cm}^{-3}$  were measured.

Yoo et al. [107] studied the influence of Cu-rich, Cu-correct, and Cu-poor precursor on the structural and morphological properties of CZTS films. Stacked Cu, Zn, and Sn elemental precursor layers with different Cu content and various stacking sequences were prepared by RF magnetron sputtering and sulfurized at  $570\text{ }^\circ\text{C}$  under S vapor.  $\text{Cu}_x\text{S}$  phase was observed in the films with precursors containing excess Cu and stoichiometric amount of Cu, but was free from such impurity phases in films produced from Cu-poor precursor. Also, a smoother morphology was obtained for the Cu-poor films.

Liu et al. [108] have reported on a single-step CZTS film fabrication approach by DC reactive sputtering. A Cu-Zn-Sn alloy target with stoichiometric Cu:Zn:Sn molar ratio of 2:1:1 and  $98\%$   $\text{H}_2\text{S}$  was used as the reactive gas for sputtering. The substrate was held at  $500\text{ }^\circ\text{C}$  during the film deposition. As-prepared films showed a preferential orientation along (112) plane with densely packed columnar grains. However, undesired secondary phases such as  $\text{Cu}_{2-x}\text{S}$  and  $\text{Cu}_3\text{SnS}_4$  were detected

**Fig. 2.16**  $J$ - $V$  characteristics of the CZTS cell with  $6.77\%$  efficiency prepared by co-sputtering and (inset) IPCE curve of the corresponding device [59]





in the film alongside CZTS. The films exhibited p-type conductivity with a carrier concentration of  $2.2 \times 10^{18} \text{ cm}^{-3}$ .

Momose et al. [101] reported on a CZTS solar cell with 3.7 % device efficiency prepared by co-sputtering of elemental metal precursors from a single target followed by sulfurization. The target was constructed by placing Zn and Sn plates on a Cu disk, exposing the top surfaces of each metal according to the required stoichiometry. The best cell was obtained by sulfurization of the deposited precursor for 7 min at 590 °C under 1.5 atmospheric pressure of S vapor. A  $V_{OC}$  of 425 mV,  $J_{SC} = 16.5 \text{ mA/cm}^2$ , and a fill factor of 53 % were recorded for the best performing cell with a SLG/MO/CZTS/CdS/In<sub>2</sub>O<sub>3</sub> device configuration. The absorber layer of the corresponding device showed a Cu-poor and Zn-rich composition with Cu/(Zn + Sn) = 0.89 and Zn/Sn = 1.15. Chalapathy et al. [99] used DC sputtering to deposit Cu/ZnSn/Cu stacked layer on Mo-coated SLG substrate at room temperature and subsequent 30 min sulfurization at 560 °C and 580 °C under S vapor to grow CZTS absorber layer. The atomic concentration of the ZnSn target was kept at Zn:Sn = 60:40. The completed device with a SLG/Mo/CZTS/CdS/i-ZnO/Al:ZnO/Al configuration prepared on the CZTS film fabricated at 560 °C showed a conversion efficiency of 4.59 % ( $V_{OC} = 545 \text{ mV}$ ,  $J_{SC} = 15.44 \text{ mA/cm}^2$ , and FF = 54.6 %). A quantum efficiency of 65 % at  $\lambda = 520 \text{ nm}$  and an optical bandgap of 1.46 eV were reported. In situ XRD and Raman data were collected during the annealing ramp-up cycle at different temperatures to understand the growth mechanism. Below 470 °C, only binary metal sulfides (Cu<sub>2-x</sub>S, ZnS, and SnS<sub>2</sub>) were observed. Kesterite CZTS compound was found to form at 470 °C. At 560 °C and 580 °C sharp CZTS peaks were observed in Raman spectra. However, small amount of Cu<sub>2-x</sub>S still exists which disappeared after 30-min annealing. Contrary to the other reports of high-efficiency CZTS(Se) solar cells, the absorber film composition in this study was highly Cu-depleted and excess in zinc. The corresponding elemental ratios were measured to be 0.67 and 1.45 for Cu/(Zn + Sn) and Zn/Sn, respectively. One important structural feature observed in the best absorber film in this study was the presence of a bilayer grain distribution with dense small grain microstructure near the Mo back contact and grooved larger grains on the top, similar to the observation made by Shin et al. [84] for the CZTS solar cell with 8.4 % efficiency.

Katagiri et al. [106] employed RF co-sputtering to fabricate CZTS thin films using Cu, ZnS, and Sn/SnS targets. The influence of the film composition was directly correlated with the photovoltaic performance of the solar cells. The compositional ratios of Cu/(Zn + Sn) and Zn/Sn were varied in a wide range from 0.75 to 1.25 and 0.8 to 1.35, respectively. The annealing was performed under N<sub>2</sub> + H<sub>2</sub>S environment at 580 °C for 3 h with different H<sub>2</sub>S concentrations from 5 to 20 %. No significant difference in the film properties were observed between the films annealed at different H<sub>2</sub>S concentrations. The device with 5 % H<sub>2</sub>S-treated absorber showed an open-circuit voltage,  $V_{OC} = 612 \text{ mV}$ , short-circuit current density,  $J_{SC} = 10.6 \text{ mA/cm}^2$ , and FF = 62.3 %, resulting in an efficiency ( $\eta$ ) of 4.1 % compared to  $V_{OC} = 634 \text{ mV}$ ,  $J_{SC} = 9.5 \text{ mA/cm}^2$ , FF = 62.7 %, and  $\eta = 3.8 \%$  of the device obtained by sulfurization under 20 % H<sub>2</sub>S concentration. To study the

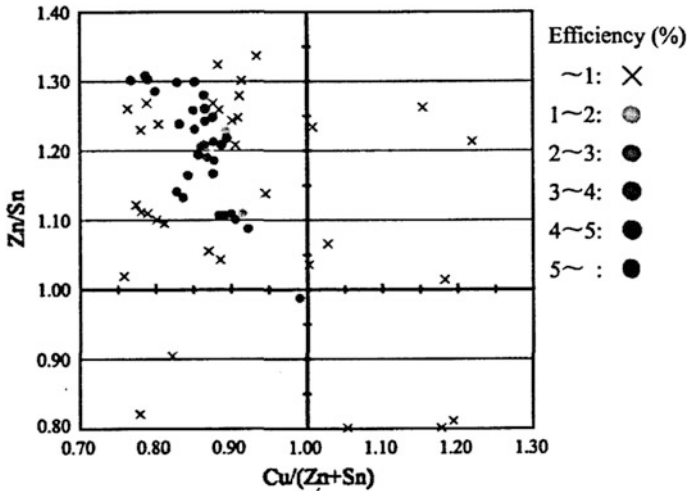


Fig. 2.17 Device efficiency versus composition of the CZTS absorber layer [106]

dependence of photovoltaic performance on the film composition, device efficiency data were plotted against the absorber layer composition, collected from a series of solar cells prepared with varying elemental ratios as shown in Fig. 2.17. Clearly, superior devices lie in a confined space within the composition map in Fig. 2.17, having a Zn/Sn ratio in the range of 1.1–1.3 and a Cu/(Zn + Sn) ratio in the range of 0.8–0.9. This study supports the observation of Cu-poor and Zn-rich stoichiometry evidenced in best performing CZTS-based devices prepared by any deposition technique and suggests the compositional range to obtain high-efficiency cells.

### 2.7.1.3 Pulsed Laser Deposition (PLD)

Pulsed laser deposition (PLD) is a relatively new method explored for the deposition of high-quality thin films and fabrication of interconnections in integrated circuits. This method offers flexible and controlled deposition of highly crystalline thin films under high vacuum with great reproducibility [110]. The film is deposited by physical ablation of the target material onto a substrate by a high-power pulsed laser radiation, and the film properties can be easily controlled by altering various deposition parameters, such as laser power, pulse rate, duration, distance from the substrate to the target, and substrate temperature. Although PLD has been proved to be a versatile and competent technique to grow different thin film materials, application of this technique for commercial manufacturing of large-area photovoltaic devices is currently limited mainly due to the small deposition area achievable by present laser technology.

In 2006, Sekiguchi et al. [111] have reported on the growth of epitaxial CZTS films on n-type (100)-oriented GaP substrates using pulsed laser deposition. CZTS

target was synthesized by solid-state reaction of equimolar amounts of  $\text{Cu}_2\text{S}$ ,  $\text{ZnS}$ , and  $\text{SnS}_2$  powders in a quartz ampoule sintered at  $750\text{ }^\circ\text{C}$  for 24 h. Deposition was carried out at a constant laser power of  $0.85\text{ J/cm}^2$  using a KrF laser source with varying substrate temperatures from  $300$  to  $400\text{ }^\circ\text{C}$ . Structural, compositional, and optical properties of the as-deposited films were reported. X-ray diffraction peaks corresponding to reflections from CZTS (112), (020)/(004), and (040)/(008) planes were observed. Films were found to be slightly S-deficient with nearly stoichiometric metal composition. Best crystallinity was obtained for the film deposited at  $400\text{ }^\circ\text{C}$  substrate temperature showing a bandgap of  $1.5\text{ eV}$ .

Photovoltaic cells employing PLD technique for absorber layer deposition were first reported by Moriya et al. in 2007 [112]. The target CZTS pellet was synthesized by adopting the similar recipe used by Sekiguchi et al. [111]. KrF excimer laser ( $248\text{ nm}$ ) with  $1.5\text{ J/cm}^2$  energy density and  $10\text{ ns}$  pulse width at a repetition rate of  $30\text{ Hz}$  was used for the deposition. CZTS film was deposited onto Mo-coated SLG substrate at room temperature and subsequently annealed under inert  $\text{N}_2$  ambient at  $300$ – $500\text{ }^\circ\text{C}$  for 1 h. The films annealed at  $500\text{ }^\circ\text{C}$  exhibited improved crystallinity with strong (112) orientation. XRD peaks corresponding to (112), (200), (220), and (312) planes of CZTS were identified. Contrary to the widely reported Cu-poor and Zn-rich stoichiometry for PV-grade CZTS films, all films under this study showed Cu-poor, Sn-rich, and S-poor stoichiometry with elemental ratios of  $\text{Zn/Sn} = 0.86$ ,  $\text{Cu}/(\text{Zn} + \text{Sn}) = 0.73$ , and  $\text{S/metal} = 0.92$  for the film annealed at  $500\text{ }^\circ\text{C}$ . The best device was obtained from the film annealed at  $500\text{ }^\circ\text{C}$ . The resulting solar cell showed  $V_{\text{OC}} = 546\text{ mV}$ ,  $J_{\text{SC}} = 6.78\text{ mA/cm}^2$ , and  $\text{FF} = 48\%$ , leading to a conversion efficiency of  $1.74\%$ .

Later in 2008, the same group of researchers changed the annealing environment from  $\text{N}_2$  to  $\text{N}_2 + \text{H}_2\text{S}$  ( $5\%$ ) in order to improve the S content of the CZTS films [113]. Also, the laser power was varied from  $0.7$  to  $1.5\text{ J/cm}^2$  to optimize the ablation process. Films deposited at  $1.5\text{ J/cm}^2$  incident laser power showed formation of Cu–Sn–S grains on the film surface, while a smoother and better quality film was obtained at  $0.7\text{ J/cm}^2$  incident laser power. As a result of annealing in the presence of  $\text{H}_2\text{S}$ , the films became nearly stoichiometric. However, the cell performance was inferior compared to the earlier report [112]. The best solar cell efficiency of  $0.64\%$  was reported with  $V_{\text{OC}}$  of  $336\text{ mV}$ ,  $J_{\text{SC}} = 6.53\text{ mA/cm}^2$ , and a fill factor of  $46\%$ .

The influence of incident laser power on the resulting CZTS film properties was further studied in detail by Pawar et al. [114]. The density of laser energy was varied from  $1.0$  to  $3.0\text{ J/cm}^2$ , and corresponding structural, morphological, and optical properties of the films were investigated. Preparation of CZTS target was similar to that of the earlier reports by Moriya et al. [113]. A KrF excimer laser source ( $248\text{ nm}$ ) operated at  $25\text{ ns}$  pulse width at a frequency of  $10\text{ Hz}$  was used to deposit CZTS thin films on glass substrates. As-deposited films were annealed under  $\text{N}_2 + \text{H}_2\text{S}$  ( $5\%$ ) ambient at  $400\text{ }^\circ\text{C}$  for 1 h. Structural, morphological, and optical properties of the as-deposited films improved with increased laser power up to  $2.5\text{ J/cm}^2$ , but degraded at higher energy density of  $3.0\text{ J/cm}^2$ . Improvement of crystallinity was evidenced from the evolution of larger diffraction peak intensity

with increasing power till  $2.5 \text{ J/cm}^2$ , which slightly decreased at  $3.0 \text{ J/cm}^2$ . A consistent enhancement of grain size and a decrease in optical bandgap were observed with higher laser energy. However, the bandgap increased slightly when the laser power increased beyond  $2.5 \text{ J/cm}^2$ .

Influence of the substrate temperature on the resulting film properties was carried out by Sun et al. [115]. Only the substrate temperature ( $T_{\text{sub}}$ ) was varied from 300 to 450 °C without changing other deposition parameters. As-deposited films were characterized for structural, optical, and compositional analysis. All CZTS films showed kesterite structure with strong (112) orientation and had a Cu-rich and S-deficient composition. At lower temperatures, isolated island-like crystallites were formed, whereas larger clusters were formed at higher temperature due to higher surface mobility leading to coalescence of islanded structures. Raman spectroscopy showed formation of  $\text{Cu}_{2-x}\text{S}$  compound at 350 and 400 °C, which disappeared at higher deposition temperature. A gradual decrease of the bandgap from 1.98 to 1.53 eV was observed with increasing  $T_{\text{sub}}$ . From XRD and Raman analysis, the authors suggested existence of internal compressive strain in the as-deposited films.

The research group of Moholkar et al. [116–118] made consistent progress over last few years on the development of CZTS solar cells made by PLD technique. Without altering the device architecture and the target synthesis recipe, a gradual improvement of efficiency was achieved by optimization of the absorber layer properties and the deposition process parameters. In 2011, they studied the influence of pulse frequency on the film properties and a conversion efficiency of 2.02 % was reported [117]. The pulse repetition rate was modulated from 2 to 20 Hz with a constant laser power of  $1.5 \text{ J/cm}^2$ . As-deposited films were annealed in  $\text{N}_2 + \text{H}_2\text{S}$  (5 %) at 400 °C for 1 h. Annealed films showed improved crystallinity with increasing pulse rate with strong (112) orientation. Thickness of the deposited films also increases up to 18 Hz, but noticed to fall at 20 Hz. Composition of the annealed films deposited at 10 Hz pulse frequency was nearly stoichiometric with Cu:Zn:Sn:S = 2.04:0.8:1.0:4.16. The optical bandgap of the films after annealing was in the range of 1.5–1.8 eV. Solar cell with a glass/Mo/CZTS/CdS/Al:ZnO/Al device structure fabricated with the absorber layer deposited at 10 Hz exhibited  $V_{\text{OC}} = 585 \text{ mV}$ ,  $J_{\text{SC}} = 6.74 \text{ mA/cm}^2$ , and a fill factor of 51 %, resulting in an efficiency of 2.02 %. A maximum 32 % quantum efficiency was recorded at  $\lambda = 530 \text{ nm}$ .

In the same year, an enhanced efficiency of 3.14 % was reported for pulsed laser deposited CZTS solar cells [116]. CZTS absorber film deposition was carried out at a fixed laser power of  $2.5 \text{ J/cm}^2$  pulsed at 10 Hz with varying deposition time from 5 to 45 min. The best device prepared with an absorber layer thickness of  $\sim 2.9 \mu\text{m}$  obtained by 30 min of deposition followed by 1 h of annealing at 400 °C under 5 %  $\text{H}_2\text{S}$  showed  $V_{\text{OC}} = 651 \text{ mV}$ ,  $J_{\text{SC}} = 8.76 \text{ mA/cm}^2$ , and  $\text{FF} = 55 \%$ , yielding an efficiency of 3.14 %. An optical bandgap of 1.54 eV for the absorber and a peak quantum efficiency of 34 % at 530 nm were measured for the respective device.

In 2012, the photoconversion efficiency was further improved to 4.13 % by optimization of chemical composition of the deposited CZTS films [118]. So far, it

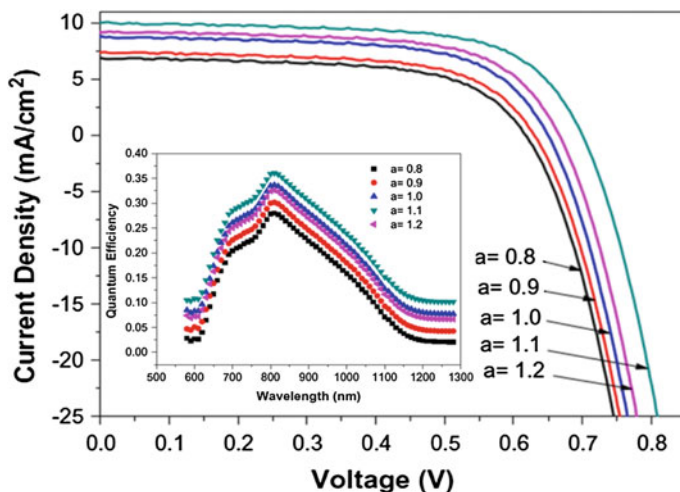


**Fig. 2.18**  $J$ - $V$  characteristics of the CZTS solar cells obtained by PLD technique deposited with various target compositions of  $a = \text{Cu}/(\text{Zn} + \text{Sn}) = 0.8$ – $1.2$  and (*inset*) the quantum efficiency curves of the respective devices [118]

is the highest efficiency CZTS-based device obtained by PLD technique. The composition ratio of  $\text{Cu}/(\text{Zn} + \text{Sn})$  in the target material was varied from 0.8 to 1.2, keeping a constant  $\text{Zn}/\text{Sn}$  ratio. The  $J$ - $V$  characteristics of the best devices obtained from CZTS films deposited using different chemical composition of the target are shown in Fig. 2.18, where “ $a$ ” denotes the  $\text{Cu}/(\text{Zn} + \text{Sn})$  ratio of the target material.

It was found that the chemical composition of the deposited films can be gradually varied by changing the composition of the target. Crystallinity of the films was improved and larger grains were obtained by increasing  $\text{Cu}/(\text{Zn} + \text{Sn})$  ratio from 0.8 to 1.1, indicating promotion of grain growth under Cu-rich and Zn-poor condition. However, structural and morphological degradation is observed for higher  $\text{Cu}/(\text{Zn} + \text{Sn})$  ratio of 1.2. The absorber layer thickness was found to increase with increasing  $\text{Cu}/(\text{Zn} + \text{Sn})$  ratio up to 1.1. Bandgap ( $E_g$ ) of the films shifted to lower energy, changing from 1.79 to 1.53 eV for increased  $\text{Cu}/(\text{Zn} + \text{Sn})$  from 0.8 to 1.2. The champion cell obtained from a target composition of  $\text{Cu}/(\text{Zn} + \text{Sn}) = 1.1$  corresponding to the absorber with  $E_g = 1.54$  eV showed  $V_{\text{OC}} = 700$  mV,  $J_{\text{SC}} = 10.01$  mA/cm<sup>2</sup>, FF = 0.59, and  $\eta = 4.13$  %. The maximum quantum efficiency of the champion cell was measured to be 36 % at 810 nm.

### 2.7.2 Non-vacuum Deposition Methods

The PVD technique is expensive and challenging to scale up because of film non-uniformity and low material utilization. Sputtering techniques are suitable for large-area deposition; however, they require expensive vacuum equipment and

sputtering targets. The PLD technique is also very expensive and has not demonstrated high-efficiency devices yet. Some of the many disadvantages of vacuum technology are complicated instrumentation, materials waste, high cost per surface area of deposition, and instability of some compounds at the high deposition temperature. Recently, the record efficiency of 11.1 %-CZTS(Se) thin film solar cell has been achieved by a non-vacuum hybrid solution-particle processing technique developed by IBM [24]. In the past decade, various non-vacuum deposition techniques have been investigated to prepare CZTS-based solar absorbers and photovoltaic solar cell fabrication including electrochemical deposition, hybrid solution-particle processing, nanoparticle-based synthesis, sol-gel spin coating, spray pyrolysis, chemical bath deposition (CBD), open-atmosphere chemical vapor deposition (OACVD), successive ion layer adsorption and reaction (SILAR), and screen printing. In this section, different non-vacuum approaches for CZTS(Se) absorber fabrication are discussed.

### 2.7.2.1 Nanocrystal-Based Approach

Recent developments of semiconductor nanoparticle synthesis have opened up new opportunities to fabricate thin films using the nanocrystals and construct solar cells with novel device architecture. Owing to tunable optoelectronic properties and easy composition control capability, nanocrystal-based approach for solar absorber fabrication is an attractive choice. In recent years, a significant research effort has been dedicated for the synthesis of I-III-VI<sub>2</sub> nanocrystals for photovoltaic applications [119–122].

In 2009, three individual research groups reported on the synthesis of CZTS nanocrystals, out of which two reported on solar cell properties, prepared using the nanocrystals [123–125]. All of these reports investigated solution-based colloidal hot-injection method for nanocrystal synthesis.

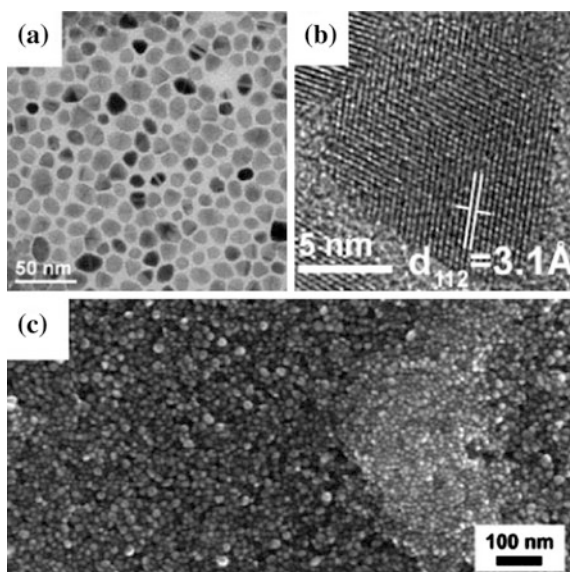
Riha et al. [125] synthesized homogeneous, nearly monodisperse CZTS nanocrystals and characterized their structural, compositional, and optical properties. Stoichiometric amounts of metal salts (copper(II) acetylacetonate, zinc acetate, and tin(IV) acetate) dissolved in oleylamine and elemental sulfur powder separately mixed in oleylamine were used as precursor solutions. Both precursors were quickly injected into trioctylphosphine oxide (TOPO) solution heated to 300 °C, initiating the nucleation and growth of CZTS nanocrystals. As-synthesized triangular and round-shaped nanocrystals were stoichiometric in composition and showed single-crystalline tetragonal structure with an average diameter of  $12.8 \pm 1.8$  nm. Diffraction spots corresponding to (112), (200), (220), (312), (008), and (332) planes of kesterite CZTS phase were identified from selected-area electron diffraction (SAED) pattern. Phase purity of the nanocrystals was further confirmed by differential thermal analysis (DTA). The CZTS nanocrystals exhibited an optical bandgap of 1.5 eV.

Sheinhagen et al. [123] reported photovoltaic properties of devices prepared using CZTS nanocrystals synthesized by arrested precipitation at high temperature.

Copper acetylacetonate, zinc acetate, tin chloride dihydrate, and elemental sulfur were used as precursor materials. Oleylamine was solely used as the coordinating solvent for the precursors. Nanocrystal growth was carried out for 1 h under an inert atmosphere at elevated precursor solution temperature of  $280^\circ\text{C}$ . As-synthesized irregular-shaped CZTS nanocrystals had an average particle size of  $10.6 \pm 2.9$  nm with slightly Sn-rich and S-poor stoichiometry. An optical bandgap of 1.3 eV was estimated and powder XRD pattern revealed characteristic peaks of kesterite CZTS structure. TEM and SEM micrographs of the as-prepared CZTS nanocrystals are shown in Fig. 2.19. The nanocrystals dispersed in toluene were used as an ink to deposit CZTS absorber layer by spray coating. A solar cell fabricated with SLG/Au/CZTS/CdS/ZnO/ITO configuration exhibited an open-circuit voltage,  $V_{\text{OC}} = 321$  mV, short-circuit current density,  $J_{\text{SC}} = 1.95$  mA/cm<sup>2</sup>, and a fill factor of 37 %, yielding an efficiency of 0.23 %.

Guo et al. [124] fabricated CZTSSe solar cells by drop-casting of CZTS nanocrystals prepared by a hot-injection method followed by selenization of the films under Se vapor. Copper(II) acetylacetonate, zinc acetylacetonate, tin(IV) bis (acetylacetonate) dibromide, and elemental sulfur at 2:1:1:4 molar ratios were used as precursors and oleylamine as the solvent for nanocrystal synthesis. The growth reaction was initiated by swift injection of the sulfur solution into the mixed metal precursor solution at  $225^\circ\text{C}$ , and the reaction was continued for 30 min. As-grown nanocrystals were purified by successive precipitation and decantation using organic solvents. Absorber film was fabricated by drop-casting of the CZTS nanocrystal ink on Mo-coated SLG substrate forming  $\sim 0.75$   $\mu\text{m}$  thick film. A thicker film was obtained by repeating the drop-casting process two times and

**Fig. 2.19** **a** TEM image of the as-synthesized CZTS nanocrystals, **b** high-resolution TEM image of a single nanocrystal, and **c** SEM image of the dispersed CZTS nanocrystals [123]



each layer was annealed under Ar at 350 °C for 1 h, removing any organic ligands attached to the nanocrystal surface. As-prepared CZTS films were further annealed under Se vapor at 400–500 °C to form CZTSSe absorber layer used for final device fabrication. Powder XRD pattern of the as-synthesized CZTS nanocrystals showed a kesterite structure with lattice parameters of  $a = 5.421 \text{ \AA}$  and  $c = 10.816 \text{ \AA}$ . A Cu-rich and Zn-poor stoichiometry was observed from EDX measurement. The size range of the nanocrystals was between 15 and 25 nm, and the bandgap was measured to be 1.5 eV. Solar cell with a SLG/Mo/CZTS<sub>x</sub>Se<sub>1-x</sub>/CdS/i-ZnO/ITO configuration obtained using the CZTS film selenized at 500 °C showed the best power conversion efficiency of 0.74 % with  $V_{OC} = 210 \text{ mV}$ ,  $J_{SC} = 11.5 \text{ mA/cm}^2$ , and a fill factor of 33.1 %.

Following the same approach, later in 2010, Guo et al. [18] made a significant improvement of the solar cell performance, reporting 7.23% photoconversion efficiency by optimizing the composition of CZTS nanocrystals.

A Cu-poor and Zn-rich composition of the nanocrystals was achieved by adjusting the amounts of metal salts in the precursor (1.332 mmol, 0.915 mmol, and 0.75 mmol for Cu, Zn, and Sn, respectively) keeping the synthesis methodology essentially same as before [124]. Absorber layer of  $\sim 1 \mu\text{m}$  was deposited on Mo-coated SLG substrate by knife-coating of the nanocrystal ink prepared by dispersion of the purified nanocrystals in hexanethiol. Selenization of the as-deposited CZTS film was carried out in the presence of Se vapor at 500 °C for 20 min, forming CZTSSe film with large, densely packed grains. Selenized films used for cell fabrication exhibited a Cu-poor and Zn-rich stoichiometry with compositional ratios of  $\text{Cu}/(\text{Zn} + \text{Sn}) = 0.79$  and  $\text{Zn}/\text{Sn} = 1.11$ . The best solar cell fabricated with a device configuration of SLG/Mo/CZTS<sub>x</sub>Se<sub>1-x</sub>/CdS/i-ZnO/ITO/Ni/Al showed  $V_{OC} = 420 \text{ mV}$ ,  $J_{SC} = 30.4 \text{ mA/cm}^2$ ,  $\text{FF} = 52.7 \%$ , and a total area efficiency of 6.73 % which was further improved to 7.23 % ( $V_{OC} = 430 \text{ mV}$ ,  $J_{SC} = 31.2 \text{ mA/cm}^2$ ,  $\text{FF} = 53.9 \%$ ) after 15-min light soaking under AM 1.5 G

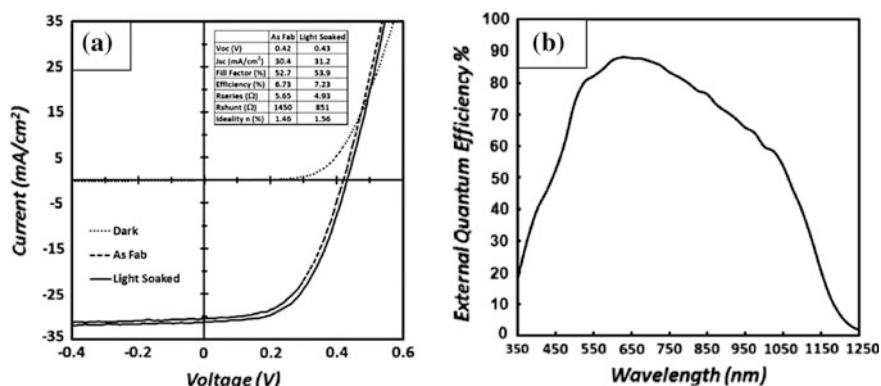


**Fig. 2.20** **a**  $J$ - $V$  characteristics of the best CZTSSe solar cell without and with 15-min light soaking and **b** external quantum efficiency of the corresponding device [18]



illumination (Fig. 2.20). The device showed  $\sim 90\%$  quantum efficiency in the visible spectrum corresponding to a bandgap of 1.05 eV.

The photoconversion efficiency was further improved to 8.5 % by Cao et al. at DuPont [126]. Binary and ternary metal sulfide nanoparticles, such as copper-tin-sulfide (CTS), ZnS, SnS, and  $\text{Cu}_x\text{S}_y$ , were synthesized by reacting metal-oleylamine complexes with sulfur in a solution of oleylamine and TOPO at high temperature ( $>200^\circ\text{C}$ ). As-synthesized metal chalcogenide nanocrystals mixed with desired proportions and dispersed in hexanethiol were used as the precursor ink for CZTSSe absorber film fabrication by spin coating. This method allowed easy composition control of the final film by changing the ratio of different metal sulfide nanocrystals in the precursor ink. Spin-coated films were annealed under Se vapor at  $560^\circ\text{C}$  for 20 min to form a robust CZTSSe absorber layer. The best solar cell with a device configuration of SLG/Mo/CZTSSe/CdS/i-ZnO/ITO/Ag showed a  $V_{\text{OC}} = 451\text{ mV}$ ,  $J_{\text{SC}} = 29.0\text{ mA/cm}^2$ , and  $\text{FF} = 64.9\%$  and a photoconversion efficiency of 8.5 % without any antireflection coating. The CTS and ZnS nanoparticles used in preparing the precursor ink for absorber layer formation are shown in Fig. 2.21a. Cross-sectional SEM revealed a bilayer microstructure of the CZTSSe absorber comprising of a fine-grained bottom layer near the back contact and the top layer consisting of larger grains (Fig. 2.21b). Similar bimodal structure was observed for high-efficiency solar cells prepared by vacuum-based thermal evaporation and DC sputtering techniques [84, 99]. The carbon-rich nanometer-sized grains in the bottom layer were the incompletely selenized initial precursor film. The micrometer-sized highly crystalline and densely packed larger grains on top were formed as a result of selenization and were carbon free. The elemental composition of the larger grain CZTSSe was estimated to be  $\text{Cu}_{1.7}\text{Zn}_{1.2}\text{SnS}_{0.6}\text{Se}_{5.0}$ . The authors suggested that highly crystalline top layer contributed to high photogeneration of carriers and the bottom carbon-rich layer acted as a low resistive interface to the Mo back contact, resulting in superior device performance. This is the best performing CZTSSe device obtained by nanocrystal-based approach.

Kameyama et al. carried out the hot-injection synthesis at various temperatures to assess the effect of temperature on the growth and crystallization of CZTS

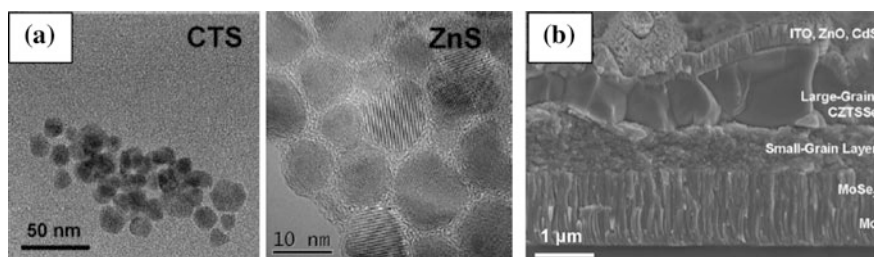


**Fig. 2.21** a TEM images of the as-synthesized copper-tin-sulfide and ZnS nanocrystals and b cross-sectional SEM image of the completed device structure [126]

nanocrystals. Metal acetate salts and elemental sulfur in oleylamine were used as the precursors [127]. At growth temperature below 180 °C, secondary CuS phase was detected, whereas pure CZTS nanocrystals were formed at temperature above 240 °C. Contrary to the general growth statistics observed for semiconductor nanocrystals grown in colloidal solution, size of the nanocrystals under this study was found to decrease at increased reaction temperature with average particle diameter of  $\sim 6.6 \pm 1.5$  nm at 120 °C,  $6.6 \pm 1.3$  nm at 180 °C,  $5.6 \pm 1.2$  nm at 240 °C, and  $5.1 \pm 1.2$  nm at 300 °C. Photoelectrochemical characterization of immobilized layer-by-layer deposited CZTS nanocrystals on ITO-coated glass exhibited p-type nature. Comparable to the bulk counterpart, a bandgap of 1.5 eV was estimated for the as-prepared nanocrystals showing no quantum confinement effect. The conduction band edge ( $E_{CB}$ ) and the valence band edge ( $E_{VB}$ ) potentials of the CZTS nanocrystals were estimated to lie at +0.3 and -1.2 eV, measured against a saturated Ag/AgCl electrode.

Riha et al. [128] fabricated a CZTS-based photoelectrochemical cell following the hot-injection synthesis technique reported earlier. Stoichiometric and Zn-rich CZTS thin films were prepared by dip coating the FTO substrates in respective nanocrystal solutions. As-deposited films were annealed in Ar atmosphere at 350 °C for 1.5 h. A redox electrolyte containing  $\text{Eu}^{3+}$  was used for the cell fabrication. Incident photon to current efficiency (IPCE) of 1.8 and 2.8 % at 500 nm was recorded for the as-deposited films prepared from stoichiometric and Zn-rich nanoparticles, respectively, which were further improved to 3.1 and 10.1 % after annealing.

Shavel et al. [129] prepared CZTSe ( $\text{Cu}_2\text{Zn}_x\text{Sn}_y\text{Se}_{1+x+2y}$ ) nanocrystals for the first time via hot-injection colloidal synthetic route by reacting amine complexes of the metal salts with elemental Se in trioctylphosphine (TOP). The synthesized nanocrystals were nearly monodisperse with an average particle size of  $20 \pm 2$  nm, showing highly faceted polyhedral geometries (Fig. 2.22a). X-ray diffraction analysis revealed a tetragonal stannite structure ( $I\bar{4}2m$ ) and compositional analysis

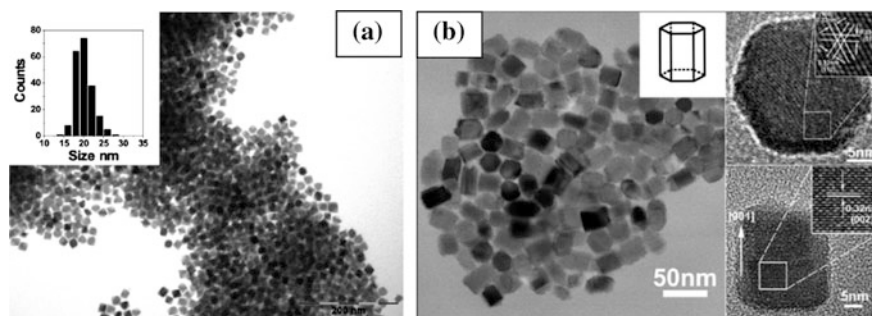


**Fig. 2.22** **a** TEM image of stannite CZTSe nanocrystals grown via hot-injection method at 295 °C for 5 min [129]; **b** TEM and HRTEM images of wurtzite CZTS nanocrystals prepared in dodecanethiol and oleylamine [130]

showed a homogeneous elemental distribution with Zn-poor and Sn-poor stoichiometry.

In general, CZTS has been reported to crystallize in tetragonal kesterite and stannite structures. Lu et al. reported CZTS nanocrystals with a new wurtzite phase, synthesized by a hot-injection method [130]. Metal–thiolate complexes prepared by dissolving metal salts in dodecanethiol were reacted with elemental sulfur in oleylamine or oleic acid at 240 °C for 1 h to grow the CZTS nanocrystals. The authors implied that dodecanethiol plays a key role in balancing the reactivities of different cations in the reaction mixture and promoted wurtzite phase CZTS growth. The new wurtzite phase CZTS nanocrystals showed a highly crystalline hexagonal structure (Fig. 2.22b), and the bandgap was measured to be 1.4 eV.

Dai et al. [131] investigated a solvothermal route for the synthesis of compositionally tunable  $(\text{Cu}_2\text{Sn})_{x/3}\text{Zn}_{1-x}\text{S}$  ( $0 \leq x \leq 0.75$ ) nanocrystals. The obtained nanocrystals showed a sphalerite structure with tunable bandgap from 3.48 to 1.23 eV. As-prepared CZTS nanocrystals with a chemical composition of  $(\text{Cu}_2\text{Sn})_{0.01}\text{Zn}_{0.97}\text{S}$  were used as the photoactive agent in a quantum dot-sensitized solar cell structure. An open-circuit voltage,  $V_{\text{OC}} = 283$  mV, a short-circuit current density,  $J_{\text{SC}} = 0.36$  mA/cm<sup>2</sup>, a fill factor of 28.6 %, and a photoconversion efficiency of 0.03 % were reported.

Cao et al. [132] also investigated a solvothermal method to synthesize CZTS nanocrystals.  $\text{CuCl}_2$ ,  $(\text{CH}_3\text{CO}_2)_2\text{Zn}$ ,  $\text{SnCl}_4$ , and sulfur were autoclaved in ethylenediamine at 180 °C for 15 h to obtain CZTS nanocrystals with 5–10 nm diameter. As-synthesized nanocrystals showed a bandgap of 1.5 eV with slightly Cu-poor, Sn-rich, and S-deficient composition. However, wurtzite ZnS phase was detected along with kesterite CZTS crystals which was removed by annealing the nanocrystal thin film under Ar + H<sub>2</sub>S (5 %) atmosphere at 550 °C for 1 h, resulting in improved crystallinity.

Single-crystalline CZTS and CZTSe nanowires have been fabricated by Shi et al. [133] using an anodic aluminum oxide (AAO) template. AAO templates (200 nm pore diameter) were immersed in the precursor solution containing metal chloride salts and sulfur/selenium in anhydrous ethylenediamine and successively autoclaved at 230 °C for 70 h to grow the nanowires. Highly ordered template-directed several micrometer-long nanowires were obtained with predominant growth direction along [110, 111] (Fig. 2.23). As-grown CZTS nanocrystals showed kesterite structure with a near-stoichiometric composition ratio of Cn:Zn:Sn:S = 2.2:0.9:0.8:4.1. An optical bandgap of ~1.5 eV for CZTS and ~1.3 eV for CZTSe nanowires was determined. This investigation showed possibility of designing and fabrication of three-dimensional CZTS solar cells using nanowires. However, CZTS nanowire-based photovoltaic device has not been reported.

### 2.7.2.2 Processing of Hydrazine-Based Solution-Particle

At IBM, Todorov et al. [134] developed a hydrazine-based hybrid solution-particle processing technique for CZTS(Se) film fabrication. A hybrid solution-particle

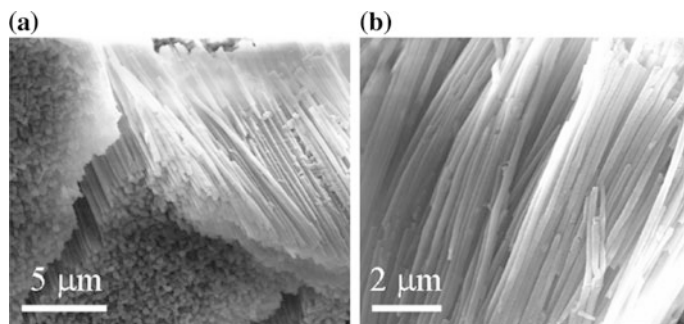


**Fig. 2.23** SEM micrographs of the as-prepared CZTS nanowires: **a** Top view and **b** side view after etching the AAO template using NaOH [133]

slurry containing copper-tin-chalcogenide mixed in hydrazine and  $\text{ZnSe}(\text{N}_2\text{H}_4)$  or  $\text{ZnS}(\text{N}_2\text{H}_4)$  was deposited layer by layer via spin coating and successively annealed at  $540^\circ\text{C}$  to form the absorber layer. By varying the amount of chalcogens, highly Se-rich, mixed sulfoselenide, and pure sulfide (Se free) absorbers were prepared.

A Zn-rich and Cu-poor stoichiometry was maintained for the films with the composition ratios of  $\text{Cu}/(\text{Zn} + \text{Sn}) = 0.8$  and  $\text{Zn}/\text{Sn} = 1.22$ , respectively. Final films showed micrometer-scale large grains. High-efficiency device performance was reported for solar cells fabricated from sulfoselenide ( $\text{S}/\text{chalcogen} = 0.4$ ) and high Se-content ( $\text{S}/\text{chalcogen} = 0.08$ ) absorbers. A remarkable conversion efficiency of 9.66 % was achieved with the sulfoselenide absorber having  $V_{\text{OC}} = 516\text{ mV}$ ,  $J_{\text{SC}} = 28.6\text{ mA}/\text{cm}^2$ , and  $\text{FF} = 65\%$ , while the device from Se-rich absorber exhibited a conversion efficiency of 9.30 % with  $V_{\text{OC}} = 412\text{ mV}$ ,  $J_{\text{SC}} = 36.4\text{ mA}/\text{cm}^2$ , and  $\text{FF} = 62\%$  (Fig. 2.24a). An optical bandgap of 1.0 eV for Se-rich sample and 1.2 eV for the sulfoselenide sample was estimated from the corresponding IPCE data (Fig. 2.24b).

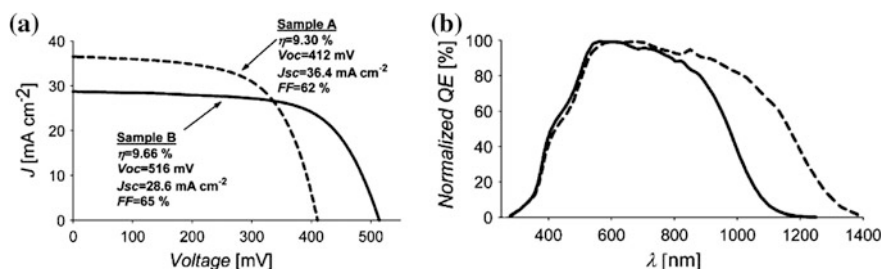
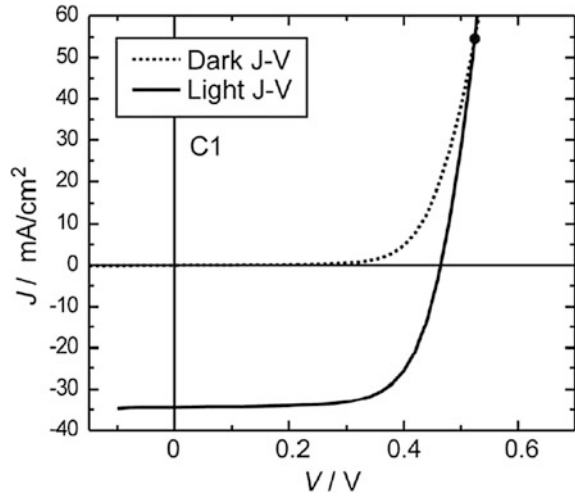


**Fig. 2.24** **a**  $J$ - $V$  characteristics of solar cells prepared from highly Se-rich (sample A) and sulfoselenide (sample B) CZTSSe absorbers and **b** normalized quantum efficiency of the corresponding devices (*dashed line* Se-rich and *straight line* sulfoselenide) [134]

**Fig. 2.25**  $J$ - $V$  characteristics of the benchmark CZTSSe device with 11.1 % efficiency [24]



Shortly after this report, the same group of researchers improved the device efficiency above 10 % following the same approach [135]. The enhanced cell performance was attributed to improved short-circuit current density and fill factor. The best solar cell exhibited an open-circuit voltage,  $V_{OC} = 517$  mV, short-circuit current density,  $J_{SC} = 6$  mA/cm<sup>2</sup>, FF = 63.7 %, leading to a photoconversion efficiency of 10.1 % corresponding to an absorber bandgap of 1.15 eV.

The benchmark CZTS-based solar cell exceeding 11 % power conversion efficiency was reported by the same group of researchers following the hydrazine-based hybrid solution-particle processing route developed earlier [24]. The enhancement of efficiency was mainly attributed to the improved short-circuit current density and fill factor. CZTSSe films with thickness of 1.5–2.2  $\mu\text{m}$  were fabricated. Larger grains with the dimension of entire absorber layer thickness were observed with a thin ( $\sim 200$  nm)  $\text{MoSe}_2$  interfacial layer at the Mo back contact. Completed device stack had a glass/Mo/CZTSSe/CdS/ZnO/ITO/Ni–Al structure with 0.45 cm<sup>2</sup> active area. The benchmark device showed a  $V_{OC} = 459.8$  mV,  $J_{SC} = 34.5$  mA/cm<sup>2</sup>, and FF = 69.8 %, resulting in an efficiency of 11.1 % under AM 1.5 G illumination with an antireflection coating (Fig. 2.25). This is the maximum power conversion efficiency achieved with kesterite CZTS-based devices inclusive of all deposition methods. Existence of a near-bandgap activation energy indicated that the cell performance was limited by Schottky–Read–Hall (SRH) recombination process occurring within the depletion region. Investigation of the device inhomogeneity within the active area using light beam-induced current (LBIC) measurement showed a minimal 5 % standard deviation of photo-generated current which is ascribed to the inhomogeneity of the absorber layer bandgap across the device.

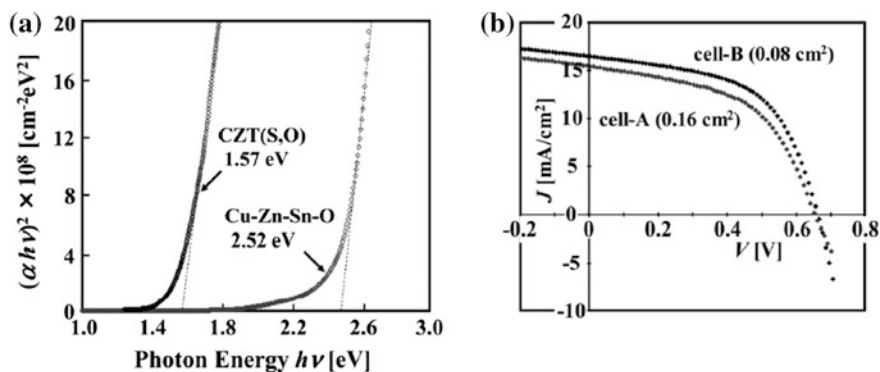


**Fig. 2.26** **a**  $(\alpha h\nu)^2$  versus  $h\nu$  plot of the as-deposited oxide precursor film and CZTS film after sulfurization and **b**  $J$ - $V$  characteristics of the champion CZTS solar cells prepared by OACVD technique [136]

### 2.7.2.3 Open-Atmosphere Chemical Vapor Deposition (OACVD)

An open-atmosphere chemical vapor deposition (OACVD) method for CZTS film fabrication has been reported by Washio et al. [136]. They reported that the CZTS thin film device with an active area of 0.08 cm<sup>2</sup> showed a  $V_{OC} = 658$  mV,  $J_{SC} = 16.5$  mA/cm<sup>2</sup>, FF = 55 %, and a power conversion efficiency of 6.03 % under AM 1.5 illumination (Fig. 2.26b).

CZTS thin films were prepared by sulfurization of an oxide precursor layer annealed at 520–560 °C under 5 % H<sub>2</sub>S for 3 h. The oxide precursor film deposited by spraying vaporized Cu(C<sub>5</sub>H<sub>7</sub>O<sub>2</sub>)<sub>2</sub>, Zn(C<sub>5</sub>H<sub>7</sub>O<sub>2</sub>)<sub>2</sub>, and Sn(C<sub>5</sub>H<sub>7</sub>O<sub>2</sub>)<sub>2</sub> sources directly onto Mo-coated SLG substrates held at 250–450 °C using N<sub>2</sub> as the carrier gas. Sulfurized CZTS films showed X-ray diffraction peaks corresponding to kesterite structure. Optical bandgap of the as-deposited oxide precursor film was 2.52 eV and decreased to 1.57 after sulfurization (Fig. 2.26a). Solar cells with a SLG/Mo/CZTS/CdS/Al:ZnO/Al device structure was fabricated. The best photovoltaic performance was obtained by the cell prepared with an absorber composition of Cu/(Zn + Sn) = 0.78 and Zn/Sn = 1.29.

### 2.7.2.4 Electrodeposition

This section presents the electrodeposition of CZTS(Se) materials. Electroplating is a potentially suitable preparation method to obtain low-cost precursor films. The electrodeposition process could provide (a) high-quality film with very low capital investment; (b) a low-cost, high-rate process; (c) use of very low-cost starting materials (e.g., low-purity salts or solvents), based on automatic purification of the deposited materials during plating; (d) a large-area, continuous, multicomponent, low-temperature deposition method; (e) deposition of films on a variety of shapes

and forms (wires, tapes, coils, and cylinders); (f) controlled deposition rates and effective material use (as high as 98 %); and (g) minimum waste generation (i.e., the solution can be recycled) [137]. The major drawback for electrodeposition is that it requires conductive substrates, which limits the application of this process in several key technologies.

Electrodeposition uses electrolysis to deposit a coating of desired form on conducting substrates from a solution (“bath”) containing the ions of interest (e.g., Cu<sup>2+</sup>, Sn<sup>2+</sup>, Zn<sup>2+</sup>). Almost without exception, one of the two phases contributing to an interface of interest in electrodeposition will be an electrolyte, which is a phase through which charge is carried by the movement of ions. The second phase at the boundary is the substrate, through which charge is carried by electronic movement. In cathodic electrodeposition, when the potential of the substrate (electrode) is moved from its equilibrium value toward negative potentials, the cation that will be reduced first is the one with the least negative (or most positive) redox potential  $E^0$ . In a solution containing Cu<sup>2+</sup>, Sn<sup>2+</sup>, and Zn<sup>2+</sup>, all three ions can be co-deposited on the surface of the substrate (cathode) when the potential is sufficiently negative. Interestingly, Se also co-deposits with Cu, Sn, and Zn under certain conditions even though it is expected to deposit on the counter electrode (anode). The conditions of electrodeposition of CZTS thin films are related to the individual electrochemical reactions that correspond with the following Nernst equation, leading to the deposition of Cu, Sn, Zn, and Se. In this case, the electrodeposition of CZTS films on the cathode is most probably caused by the combination of electrochemical and chemical reactions as follows:



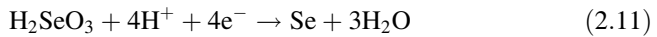
$$E = E_{Cu}^0 + RT/2F \ln [Cu^{2+}] = 0.337 + 0.0295 \log [Cu^{2+}] \quad (2.6)$$



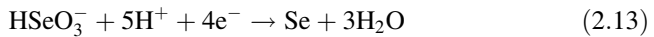
$$E = E_{Sn}^0 + RT/2F \ln [Sn^{2+}] = -0.136 + 0.0295 \log [Sn^{2+}] \quad (2.8)$$



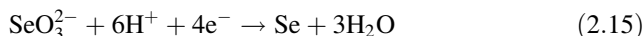
$$E = E_{Zn}^0 + RT/2F \ln [Zn^{2+}] = -0.763 + 0.0295 \log [Zn^{2+}] \quad (2.10)$$



$$E = 0.741 - 0.0591 \text{ pH} + 0.0148 \log [H_2SeO_3] \quad (2.12)$$



$$E = 0.778 - 0.0739 \text{ pH} + 0.0148 \log [\text{HSeO}_3^-] \quad (2.14)$$



$$E = 0.875 - 0.0886 \text{ pH} + 0.0148 \log [\text{SeO}_3^{2-}] \quad (2.16)$$



where  $E$  is the electrode equilibrium potential with respect to the standard hydrogen electrode (SHE) and  $E_{\text{Cu}}^0$ ,  $E_{\text{Sn}}^0$ , and  $E_{\text{Zn}}^0$  are the standard electrode potentials of Cu, Sn, and Zn, respectively.  $F$  is Faraday's constant equal to 96,485 Coulomb/mole. Concentration of  $\text{H}^+$  is converted to pH scale and shown in the equations. The logarithm of concentrations of different chemical species shifts the electrode equilibrium potential at the specific concentration.

Several research group reported successful electrodeposition of CZTS materials [138–147]. Ennaoui et al. [139] fabricated electrodeposited  $\text{Cu}_2\text{ZnSnS}_4$  device with 3.4 % efficiency, with a  $V_{\text{OC}} = 0.56$  V,  $J_{\text{SC}} = 14.8$  mA/cm<sup>2</sup>, and FF = 0.41. The absorber layers were prepared by solid-state reaction in  $\text{H}_2\text{S}$  atmosphere of electrodeposited Cu–Zn–Sn precursors. Araki et al. [140] fabricated electrodeposited  $\text{Cu}_2\text{ZnSnS}_4$  device with 3.16 % efficiency, with a  $V_{\text{OC}} = 0.54$  V,  $J_{\text{SC}} = 12.6$  mA/cm<sup>2</sup>, and FF = 0.46. The absorber layers were prepared by annealing the electrodeposited Cu–Zn–Sn precursors with sulfur in  $\text{N}_2$  atmosphere. Farinella et al. [146] reported the fabrication of quaternary  $\text{Cu}_2\text{ZnSnS}_4$  thin films on flexible ITO substrates supported by polyethylene terephthalate (PET) by co-electrodeposition of all elements from a sulfate solution potentiostatically. Bhattacharya [147] electrodeposited multilayered Cu–Sn–Zn metal films on Mo/glass substrates. Cu and Zn thin films were prepared from aqueous solution, and Sn was prepared from ionic liquid solvent. Cu/Sn/Zn stacked layers were annealed in a tube furnace in elemental sulfur and selenium at 570 °C. The device efficiency of such electrodeposited CZTSS thin film was 3.6 % with a  $V_{\text{OC}} = 0.54$  V,  $J_{\text{SC}} = 16.9$  mA/cm<sup>2</sup>, and FF = 0.40. Higher-performance  $\text{Cu}_2\text{ZnSnS}_4$  photovoltaic devices were fabricated by Ahmed et al. [138] using stacked electrodeposited Cu/Zn/Sn or Cu/Sn/Zn layers. The stacked layers were first annealed at low temperature (210–350 °C) in an  $\text{N}_2$  environment in order to produce homogeneous (Cu, Zn) and (Cu, Sn) alloys and subsequently annealed at 550–590 °C in a sulfur atmosphere for 5–15 min. The electrodeposited device (Fig. 2.27) showed a power conversion efficiency of 7.3 %, with open-circuit voltage ( $V_{\text{OC}} = 567$  mV), photocurrent ( $J_{\text{SC}} = 22$  mA cm<sup>-2</sup>), and the fill factor (FF = 58.1 %).

### 2.7.2.5 Monograin Layer Cell

Recently, a new type of device structure known as monograin layer (MGL) solar cell has emerged as a potential alternative to realize low-cost large-area



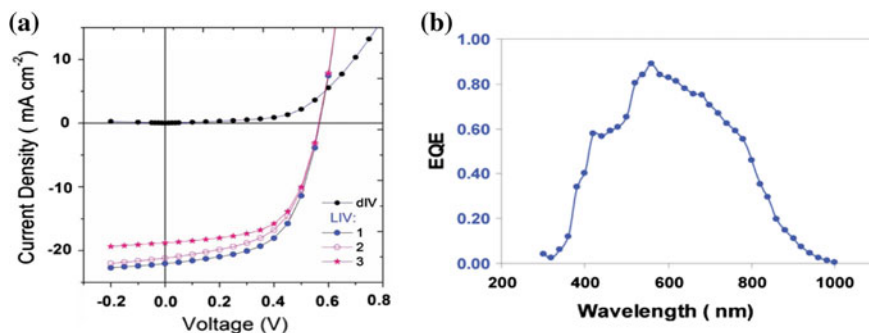


**Fig. 2.27** **a**  $I$ - $V$  characteristics of electrodeposited CZTS solar cell under *dark* (black) and 1 sun (lines 1, 2, and 3) illumination for a champion CZTS cell, showing efficiencies of 7.3, 6.74, and 6.86 %, respectively. **b** The quantum efficiency (QE) curve. LIV and dIV mean light and dark current–voltage curve, respectively [138]

photovoltaic devices [83, 148–150]. In this method, monocrystalline granular powders of the absorber material are embedded in an epoxy layer for the absorber layer fabrication. Each monocrystalline particle makes an islanded junction with the top CdS layer to form the effective heterojunction. The schematic of the MGL cell structure is depicted in Fig. 2.28a.

The monocrystalline powders are usually produced by recrystallization of binary chalcogenides:  $\text{CuS}(\text{Se})$ ,  $\text{ZnS}(\text{Se})$ , and  $\text{SnS}(\text{Se})$  in an evacuated quartz ampoule at high temperature. This device structure offers several advantages including simple and low-cost fabrication process and allows the possibility of flexible solar cells to be fabricated without degradation of the absorber layer due to mechanical stress retaining the superior optoelectronic properties of the single-crystalline absorber. Researchers at Tallinn University have pioneered this technology and prepared  $\text{Cu}_2\text{ZnSn}(\text{Se}_{1-x}\text{S}_x)_4$  solar cells with varying S/Se ratios. The best cell showed an open-circuit voltage of 622 mV, short-circuit current density of 15.87 mA/cm<sup>2</sup>, and

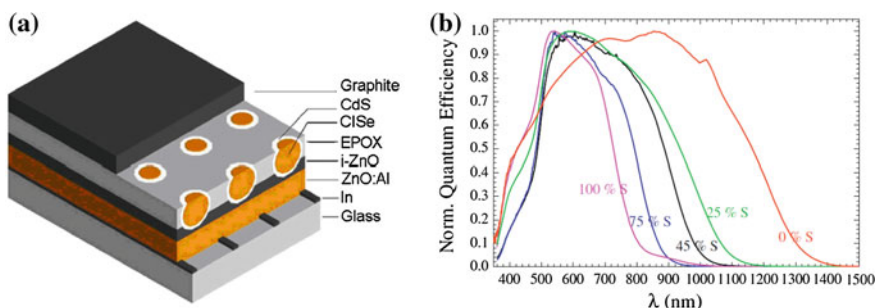


**Fig. 2.28** **a** Schematic of a monograin layer (MGL) solar cell structure [149] and **b** quantum efficiencies of MGL cells with varying S/Se ratios [148]

fill factor of 60 %, leading to an efficiency of 5.9 % with absorber layer containing 75 mol% of sulfur and 25 mol% of Se [148]. The quantum efficiencies of solar cells with different S/Se compositions are shown in Fig. 2.28b.

## References

1. Green, M.A., Emery, K., Hishikawa, Y., Warta, W., Dunlop, E.D.: Solar cell efficiency tables (version 42). *Prog. Photovoltaics Res. Appl.* **21**, 827–837 (2013)
2. Green, M.A.: Estimates of Te and In prices from direct mining of known ores. *Prog. Photovoltaics Res. Appl.* **17**, 347–359 (2009)
3. Tao, C.S., Jiang, J., Tao, M.: Natural resource limitations to terawatt-scale solar cells. *Sol. Energy Mater. Sol. Cells* **95**, 3176–3180 (2011)
4. Feltrin, A., Freundlich, A.: Material considerations for terawatt level deployment of photovoltaics. *Renew. Energy* **33**, 180–185 (2008)
5. Zuser, A., Rechberger, H.: Considerations of resource availability in technology development strategies: the case study of photovoltaics. *Resour. Conserv. Recycl.* **56**, 56–65 (2011)
6. Fthenakis, V.: Sustainability of photovoltaics: the case for thin-film solar cells. *Renew. Sustain. Energy Rev.* **13**, 2746–2750 (2009)
7. Wadia, C., Alivisatos, A.P., Kammen, D.M.: Materials availability expands the opportunity for large-scale photovoltaics deployment. *Environ. Sci. Technol.* **43**, 2072–2077 (2009)
8. Candelisea, C., Speirsa, J.F., Grossa, R.J.K.: Materials availability for thin film (TF) PV technologies development: a real concern? *Renew. Sustain. Energy Rev.* **15**, 4972–4981 (2012)
9. Green, M.A.: Consolidation of thin-film photovoltaic technology: the coming decade of opportunity. *Prog. Photovoltaics Res. Appl.* **14**, 383–392 (2006)
10. U.S. Department of Energy, *Critical Materials Strategy*, (2010)
11. European Commission, *Critical Raw Materials for the EU*, (2010)
12. O'Neill, B.: Indium market forces, a commercial perspective. In: Photovoltaic specialists conference (PVSC), 35th IEEE, pp. 000556–000559 (2010)
13. Fthenakis, V.M., Moskowitz, P.D.: Thin-film photovoltaic cells: health and environmental issues in their manufacture use and disposal. *Prog. Photovoltaics Res. Appl.* **3**, 295–306 (1995)
14. Repins, I., Beall, C., Vora, N., DeHart, C., Kuciauskas, D., Dipppo, P., To, B., Mann, J., Hsu, W.-C., Goodrich, A., Noufi, R.: Co-evaporated  $\text{Cu}_2\text{ZnSnSe}_4$  films and devices. *Sol. Energy Mater. Sol. Cells* **101**, 154–159 (2012)
15. Bag, S., Gunawan, O., Gokmen, T., Zhu, Y., Todorov, T.K., Mitzi, D.B.: Low band gap liquid-processed CZTSe solar cell with 10.1 % efficiency. *Energy Environ. Sci.* **5**, 7060–7065 (2012)
16. Oleksyuk, I.D., Gulay, L.D., Dydchak, I.V., Piskach, L.V., Parasyuk, O.V., Marchuk, O.V.: Single crystal preparation and crystal structure of the  $\text{Cu}_2\text{Zn/Cd}$ ,  $\text{Hg/SnSe}_4$  compounds. *J. Alloy. Compd.* **340**, 141–145 (2002)
17. Wang, K., Gunawan, O., Todorov, T., Shin, B., Chey, S.J., Bojarczuk, N.A., Mitzi, D., Guha, S.: Thermally evaporated  $\text{Cu}_2\text{ZnSnS}_4$  solar cells. *Appl. Phys. Lett.* **97**, 143508 (2010)
18. Guo, Q., Ford, G.M., Yang, W.-C., Walker, B.C., Stach, E.A., Hillhouse, H.W., Agrawal, R.: Fabrication of 7.2 % efficient CZTSSe solar cells using CZTS nanocrystals. *J. Am. Chem. Soc.* **132**, 17384–17386 (2010)
19. Willoughby, A.: *Solar Cell Materials: Developing Technologies*, Wiley Series in Materials for Electronic & Optoelectronic Applications, pp. 186. Wiley, Chichester (2014)
20. <http://www.webelements.com/>
21. U.S. geological survey, <http://minerals.usgs.gov/minerals/pubs/commodity/>

22. <http://www.metalprices.com/>
23. Shockley, W., Queisser, H.J.: Detailed balance limit of efficiency of p-n junction solar cells. *J. Appl. Phys.* **32**, 510 (1961)
24. Todorov, T.K., Tang, J., Bag, S., Gunawan, O., Gokmen, T., Zhu, Y., Mitzi, D.B.: Beyond 11 % efficiency: characteristics of state-of-the-Art  $\text{Cu}_2\text{ZnSn}(\text{S},\text{Se})_4$  solar cells. *Adv. Energy Mater.* **3**, 34–38 (2013)
25. Bernardini, G.P., Borrini, D., Caneschi, A., Di Benedetto, F., Gatteschi, D., Ristori, D., Romanelli, M.: EPR and SQUID magnetometry study of  $\text{Cu}_2\text{FeSnS}_4$  (stannite) and  $\text{Cu}_2\text{ZnSnS}_4$  (kesterite). *Phys. Chem. Miner.* **27**, 453–461 (2000)
26. Hall, S.R., Szymanski, J.T., Stewart, J.M.: Kesterite,  $\text{Cu}_2(\text{Zn},\text{Fe})\text{SnS}_4$ , and stannite,  $\text{Cu}_2(\text{Fe},\text{Zn})\text{SnS}_4$ , structurally similar but distinct minerals. *Can. Mineral.* **16**, 131–137 (1978)
27. Brockway, L.O.: The crystal structure of stannite  $\text{Cu}_2\text{FeSnS}_4$ . *Zeitschrift für Kristallographie—Crystalline Materials*, 89, 434–441 (1934)
28. Bonazzi, P., Bindi, L., Bernardini, G.P., Menchetti, S.: A model for the mechanism of incorporation of Cu, Fe and Zn in the stannite—kesterite series,  $\text{Cu}_2\text{FeSnS}_4$ — $\text{Cu}_2\text{ZnSnS}_4$ . *Can. Mineral.* **41**, 639–647 (2003)
29. Schorr, S.: Structural aspects of adamantine like multinary chalcogenides. *Thin Solid Films* **515**, 5985–5991 (2007)
30. Mitzi, D.B., Gunawan, O., Todorov, T.K., Wang, K., Guha, S.: The path towards a high-performance solution-processed kesterite solar cell. *Sol. Energy Mater. Sol. Cells* **95**, 1421–1436 (2011)
31. Schorr, S.: The crystal structure of kesterite type compounds: a neutron and X-ray diffraction study. *Sol. Energy Mater. Sol. Cells* **95**, 1482–1488 (2011)
32. Catlow, C.R.A., Guo, Z.X., Miskufova, M., Shevlin, S.A., Smith, A.G.H., Sokol, A.A., Walsh, A., Wilson, D.J., Woodley, S.M.: Advances in computational studies of energy materials. *Philos. Trans. Roy. Soc. A* **368**, 3379–3456 (2010)
33. Persson, C.: Electronic and optical properties of  $\text{Cu}_2\text{ZnSnS}_4$  and  $\text{Cu}_2\text{ZnSnSe}_4$ . *J. Appl. Phys.* **107**, 053710 (2010)
34. Chen, S., Gong, X.G., Walsh, A., Wei, S.-H.: Crystal and electronic band structure of  $\text{Cu}_2\text{ZnSnX}_4$  (X = S and Se) photovoltaic absorbers: first-principles insights. *Appl. Phys. Lett.* **94**, 041903 (2009)
35. Paier, J., Asahi, R., Nagoya, A., Kresse, G.:  $\text{Cu}_2\text{ZnSnS}_4$  as a potential photovoltaic material: a hybrid Hartree-Fock density functional theory study. *Phys. Rev. B* **79**, 115–126 (2009)
36. Walsh, A., Chen, S., Gong, X.G., Wei, S.H.: Crystal structure and defect reactions in the kesterite solar cell absorber  $\text{Cu}_2\text{ZnSnS}_4$  (CZTS): theoretical insights. *AIP Conf. Proc.* **1399**, 63 (2011)
37. Walsh, A., Wei, S.H., Chen, S.Y., Gong, X.G.: Design of quaternary chalcogenide photovoltaic absorbers through cation mutation. In: 34th IEEE Photovoltaic Specialists Conference, 1–3, pp. 1803–1806 (2009)
38. Walsh, A., Chen, S., Wei, S., Gong, X.: Kesterite thin film solar cells: advances in materials modelling of  $\text{Cu}_2\text{ZnSnS}_4$ . *Adv. Energy Mater.* **2**, 400–409 (2012)
39. Zhang, Y., Sun, X., Zhang, P., Yuan, X., Huang, F., Zhang, W.: Structural properties and quasiparticle band structures of Cu-based quaternary semiconductors for photovoltaic applications. *J. Appl. Phys.* **111**, 063709 (2012)
40. Raulot, J.M., Domain, C., Guillemoles, J.F.: Ab initio investigation of potential indium and gallium free chalcopyrite compounds for photovoltaic application. *J. Phys. Chem. Solids* **66**, 2019–2023 (2005)
41. Nozaki, H., Fukano, T., Ohta, S., Seno, Y., Katagiri, H., Jimbo, K.: Crystal structure determination of solar cell materials:  $\text{Cu}_2\text{ZnSnS}_4$  thin films using X-ray anomalous dispersion. *J. Alloy. Compd.* **524**, 22–25 (2012)
42. Siebentritt, S., Schorr, S.: Kesterites—a challenging material for solar cells. *Prog. Photovoltaics Res. Appl.* **20**, 512–519 (2012)

43. Chen, S., Gong, X.G., Walsh, A., Wei, S.H.: Electronic structure and stability of quaternary chalcogenide semiconductors derived from cation cross-substitution of II–VI and I–III–VI<sub>2</sub> compounds. *Phys. Rev. B* **79**, 165211 (2009)
44. Oleksyuk, I.D., Dudchar, I.V., Piskach, L.V.: Phase equilibria in the Cu<sub>2</sub>S–ZnS–SnS<sub>2</sub> system. *J. Alloy. Compd.* **368**, 135–143 (2004)
45. Dudchak, I.V., Piskach, L.V.: Phase equilibria in the Cu<sub>2</sub>SnSe<sub>3</sub>–SnSe<sub>2</sub>–ZnSe system. *J. Alloy. Compd.* **351**, 145–150 (2003)
46. Das, S., Krishna, R.M., Ma, S., Mandal, K.C.: Single phase polycrystalline Cu<sub>2</sub>ZnSnS<sub>4</sub> grown by vertical gradient freeze technique. *J. Cryst. Growth* **381**, 148–152 (2013)
47. Das, S., Mandal, K.C.: Cu<sub>2</sub>ZnSnSe<sub>4</sub> photovoltaic absorber grown by vertical gradient freeze technique. *Jpn. J. Appl. Phys.* **52**, 125502 (2013)
48. Nagoya, A., Asahi, R., Wahl, R., Kresse, G.: Defect formation and phase stability of Cu<sub>2</sub>ZnSnS<sub>4</sub> photovoltaic material. *Phys. Rev. B* **81**, 113202 (2010)
49. Chen, S.Y., Gong, X.G., Walsh, A., Wei, S.H.: *Appl. Phys. Lett.* **96**, 021902 (2010)
50. Dale, P.J., Hoesnes, K., Scragg, J., Siebentritt, S.: A review of the challenges facing kesterite based thin film solar cells. In: *Photovoltaic Specialists Conference (PVSC)*, 34th IEEE, pp. 002080–002085 (2009)
51. Maeda, T., Nakamura, S., Wada, T.: First-principles calculations of vacancy formation in In-free photovoltaic semiconductor Cu<sub>2</sub>ZnSnSe<sub>4</sub>. *Thin Solid Films* **519**, 7513–7516 (2011)
52. Gödecke, T., Haalboom, T., Ernst, F.: Phase equilibria of Cu–In–Se. I. Stable states and non-equilibrium states of the In<sub>2</sub>Se<sub>3</sub>–Cu<sub>2</sub>Se subsystem. *Zeitschrift für Metallkunde*, **91**, 622–634 (2000)
53. Chen, S., Yang, J.-H., Gong, X.G., Walsh, A., Wei, S.-H.: Intrinsic point defects and complexes in the quaternary kesterite semiconductor Cu<sub>2</sub>ZnSnS<sub>4</sub>. *Phys. Rev. B* **81**, 245204 (2010)
54. Persson, C., Lany, S., Zhao, Y.-J., Zunger, A.: n-type doping of CuInSe<sub>2</sub> and CuGaSe<sub>2</sub>. *Phys. Rev. B* **72**, 035211 (2005)
55. Maeda, T., Nakamura, S., Wada, T.: First principles calculations of defect formation in in-free photovoltaic semiconductors Cu<sub>2</sub>ZnSnS<sub>4</sub> and Cu<sub>2</sub>ZnSnSe<sub>4</sub>. *Jpn. J. Appl. Phys.* **50**, 04DP07 (2011)
56. Redinger, A., Berg, D.M., Dale, P.J., Djemour, R., Gütay, L., Eisenbarth, T., Valle, N., Siebentritt, S.: Route toward high-efficiency single-phase Cu<sub>2</sub>ZnSn(S,Se)<sub>4</sub> thin film solar cells: model experiments and literature review. *IEEE J. Photovoltaics* **1**, 200–206 (2011)
57. Redinger, A., Hönes, K., Fontané, X., Izquierdo-Roca, V., Saucedo, E., Valle, N., Pérez-Rodríguez, A., Siebentritt, S.: Detection of a sZnSe secondary phase in coevaporated Cu<sub>2</sub>ZnSnSe<sub>4</sub> thin films. *Appl. Phys. Lett.* **98**, 101907 (2011)
58. Bär, M., Schubert, B.-A., Marsen, B., Krause, S., Pookpanratana, S., Unold, T., Weinhardt, L., Heske, C., Schock, H.-W.: Impact of KCN etching on the chemical and electronic surface structure of Cu<sub>2</sub>ZnSnS<sub>4</sub> thin film solar cell absorbers. *Appl. Phys. Lett.* **99**, 152111 (2011)
59. Katagiri, H., Jimbo, K., Yamada, S., Kamimura, T., Maw, W.S., Fukano, T., Ito, T., Motohiro, T.: Enhanced conversion efficiencies of Cu<sub>2</sub>ZnSnS<sub>4</sub>-based thin film solar cells by using preferential etching technique. *Appl. Phys. Exp.* **1**, 041201 (2008)
60. Timmo, K., Altosaar, M., Raudoja, J., Grossberg, M., Danilson, M., Volobujeva, O., Mellikov, E.: Chemical etching of Cu<sub>2</sub>ZnSn(S,Se)<sub>4</sub> monograin powder. In: *Photovoltaic Specialists Conference (PVSC)*, 35th IEEE, pp. 001982–001985 (2010)
61. Fairbrother, A., García-Hemme, E., Izquierdo-Roca, V., Fontané, X., Pulgarín-Agudelo, F. A., Vigil-Galán, O., Pérez-Rodríguez, A., Saucedo, E.: Development of a selective chemical etch to improve the conversion efficiency of Zn-Rich Cu<sub>2</sub>ZnSnS<sub>4</sub> solar cells. *J. Am. Chem. Soc.* **134**, 8018–8021 (2012)
62. Biswas, K., Lany, S., Zunger, A.: The electronic consequences of multivalent elements in inorganic solar absorbers: multivalency of Sn in Cu<sub>2</sub>ZnSnS<sub>4</sub>. *Appl. Phys. Lett.* **96**, 201902 (2010)

63. Siebentritt, S., Igalson, M., Persson, C., Lany, S.: The electronic structure of chalcopyrites—bands, point defects and grain boundaries. *Prog. Photovoltaics Res. Appl.* **18**, 390–410 (2010)
64. Nagoya, A., Asahi, R., Kresse, G.: First-principles study of  $\text{Cu}_2\text{ZnSnS}_4$  and the related band offsets for photovoltaic applications. *J. Phys. Condens. Matter* **23**, 404203 (2011)
65. Chen, S., Walsh, A., Gong, X.-G., Wei, S.-H.: Classification of lattice defects in the Kesterite  $\text{Cu}_2\text{ZnSnS}_4$  and  $\text{Cu}_2\text{ZnSnSe}_4$  earth-abundant solar cell absorbers. *Adv. Mater.* **25**, 1522–1539 (2013)
66. Zhai, Y.-T., Chen, S., Yang, J.-H., Xiang, H.-J., Gong, X.-G., Walsh, A., Kang, J., Wei, S.-H.: Structural diversity and electronic properties of  $\text{Cu}_2\text{Sn}_x$  ( $X = \text{S}, \text{Se}$ ): a first-principles investigation. *Phys. Rev. B* **84**, 075213 (2011)
67. Friedlmeier, T.M., Wieser, N., Walter, T., Dittrich, H., Schock, H.W.: 14th European photovoltaic solar energy conference, vol. 1, p. 1242 (1997)
68. Tanaka, T., Nagatomo, T., Kawasaki, D., Nishio, M., Guo, Q.X., Wakahara, A., Yoshida, A., Ogawa, H.: Preparation of  $\text{Cu}_2\text{ZnSnS}_4$  thin films by hybrid sputtering. *J. Phys. Chem. Solids* **66**, 1978–1981 (2005)
69. Zhang, J., Shao, L.X., Fu, Y.J., Xie, E.Q.:  $\text{Cu}_2\text{ZnSnS}_4$  thin films prepared by sulfurization of ion beam sputtered precursor and their electrical and optical properties. *Rare Met.* **25**, 315–319 (2006)
70. Leitao, J.P., Santos, N.M., Fernandes, P.A., Salome, P.M.P., da Cunha, A.F., Gonzalez, J.C., Ribeiro, G.M., Matinaga, F.M.: Photoluminescence and electrical study of fluctuating potentials in  $\text{Cu}_2\text{ZnSnS}_4$ -based thin films. *Phys. Rev. B* **84**, 024120 (2011)
71. Ito, K., Nakazawa, T.: Electrical and optical properties of Stannite-type quaternary semiconductor thin films. *Jpn. J. Appl. Phys.* **27**, 2094–2097 (1988)
72. Nakayama, N., Ito, K.: Sprayed films of stannite  $\text{Cu}_2\text{ZnSnS}_4$ . *Appl. Surf. Sci.* **92**, 171–175 (1996)
73. Katagiri, H., Sasaguchi, N., Hando, S., Hoshino, S., Ohashi, J., Yokota, T.: Preparation and evaluation of  $\text{Cu}_2\text{ZnSnS}_4$  thin films by sulfurization of E-B evaporated precursors. *Sol. Energy Mater. Sol. Cells* **49**, 407–414 (1997)
74. Katagiri, H., Saitoh, K., Washio, T., Shinohara, H., Kurumadani, T., Miyajima, S.: Development of thin film solar cell based on  $\text{Cu}_2\text{ZnSnS}_4$  thin films. *Sol. Energy Mater. Sol. Cells* **65**, 141–148 (2001)
75. Katagiri, H., Ishigaki, N., Ishida, T., Saito, K.: Characterization of  $\text{Cu}_2\text{ZnSnS}_4$  thin films prepared by vapor phase sulfurization. *Jpn. J. Appl. Phys.* **40**, 500–504 (2001)
76. Matsushita, H., Maeda, T., Katsui, A., Takizawa, T.: Thermal analysis and synthesis from the melts of Cu-based quaternary compounds  $\text{Cu-III-IV-VI}_4$  and  $\text{Cu}_2\text{-II-IV-VI}_4$  (II = Zn, Cd; III = Ga, In; IV = Ge, Sn; VI = Se). *J. Cryst. Growth* **208**, 416–422 (2000)
77. Wibowo, R.A., Kim, W.S., Lee, E.S., Munir, B., Kim, K.H.: Single step preparation of quaternary  $\text{Cu}_2\text{ZnSnSe}_4$  thin films by RF magnetron sputtering from binary chalcogenide targets. *J. Phys. Chem. Solids* **68**, 1908–1913 (2007)
78. Wibowo, R.A., Lee, E.S., Munir, B., Kim, K.H.: Pulsed laser deposition of quaternary  $\text{Cu}_2\text{ZnSnSe}_4$  thin films. *Phys. Status Solidi A* **204**, 3373–3379 (2007)
79. Friedlmeier, T.M., Dittrich, H., Schock, H.W.: 11th international conference on ternary and multinary compounds. ICTMC-11 Institute of Physics Publishing, Salford, UK (1998)
80. Repins, I., Vora, N., Beall, C., Wei, S.-H., Yan, Y., Romero, M., Teeter, G., Du, H., To, B., Young, M., Noufi, R.: Kesterites and chalcopyrites: a comparison of close cousins. In: *MRS proceedings*, vol. 1324 (2011)
81. Schorr, S., Hoebler, H.J., Tovar, M.: A neutron diffraction study of the stannite-kesterite solid solution series. *Eur. J. Mineral.* **19**, 65–73 (2007)
82. Washio, T., Nozaki, H., Fukano, T., Motohiro, T., Jimbo, K., Katagiri, H.: Analysis of lattice site occupancy in kesterite structure of  $\text{Cu}_2\text{ZnSnS}_4$  films using synchrotron radiation X-ray diffraction. *J. Appl. Phys.* **110**, 074511 (2011)
83. Kask, E., Raadik, T., Grossberg, M., Josepson, R., Krustok, J.: Deep defects in  $\text{Cu}_2\text{ZnSnS}_4$  monograin solar cells. *Energy Procedia* **10**, 261–265 (2011)

84. Shin, B., Gunawan, O., Nestor, Y.Z., Bojarczuk, A., Chey, S.J., Guha, S.: Thin film solar cell with 8.4 % power conversion efficiency using an earth-abundant  $\text{Cu}_2\text{ZnSnS}_4$  absorber. *Prog. Photovoltaics Res. Appl.* **21**, 72–76 (2013)
85. Araki, H., Mikaduki, A., Kubo, Y., Sato, T., Jimbo, K., Maw, W.S., Katagiri, H., Yamazaki, M., Oishi, K., Takeuchi, A.: Preparation of  $\text{Cu}_2\text{ZnSnS}_4$  thin films by sulfurization of stacked metallic layers. *Thin Solid Films* **517**, 1457–1460 (2008)
86. Kobayashi, T., Jimbo, K., Tsuchida, K., Shinoda, S., Oyanagi, T., Katagiri, H.: Investigation of  $\text{Cu}_2\text{ZnSnS}_4$ -based thin film solar cells using abundant materials. *Jpn. J. Appl. Phys.* **44**, 783–787 (2005)
87. Schubert, B.-A., Marsen, B., Cinque, S., Unold, T., Klenk, R., Schorr, S., Schock, H.-W.:  $\text{Cu}_2\text{ZnSnS}_4$  thin film solar cells by fast coevaporation. *Prog. Photovoltaics Res. Appl.* **19**, 93–96 (2011)
88. Friedlmeier, T.M., Wieser, N., Walter, T., Dittrich, H., Schock, H.-W.: Heterojunctions based on  $\text{Cu}_2\text{ZnSnS}_4$  and  $\text{Cu}_2\text{ZnSnSe}_4$  thin films. In: Proceedings of the 14th European PVSEC and Exhibition, P4B.10, 1242 (1997)
89. Katagiri, H., Jimbo, K., Moriya, K., Tsuchida, K.: Solar cell without environmental pollution by using CZTS thin film. In: Proceedings of the 3rd World conference on photovoltaic energy conversion, Osaka, pp. 2874–2879 (2003)
90. Weber, A., Mainz, R., Schock, H.W.: On the Sn loss from thin films of the material system  $\text{Cu-Zn-Sn-S}$  in high vacuum. *J. Appl. Phys.* **107**, 013516 (2010)
91. Redinger, A., Berg, D.M., Dale, P.J., Siebentritt, S.: The consequences of Kesterite equilibria for efficient solar cells. *J. Am. Chem. Soc.* **133**, 3320–3323 (2011)
92. Tanaka, T., Kawasaki, D., Nishio, M., Guo, Q., Ogawa, H.: Fabrication of  $\text{Cu}_2\text{ZnSnS}_4$  thin films by co-evaporation, *physica status solidi C*. **3**, 2844–2847 (2006)
93. Oishi, K., Saito, G., Ebina, K., Nagahashi, M., Jimbo, K., Maw, W.S., Katagiri, H., Yamazaki, M., Araki, H., Takeuchi, A.: Growth of  $\text{Cu}_2\text{ZnSnS}_4$  thin films on Si (100) substrates by multisource evaporation. *Thin Solid Films* **517**, 1449–1452 (2008)
94. Tanaka, T., Yoshida, A., Saiiki, D., Saito, K., Guo, Q., Nishio, M., Yamaguchi, T.: Influence of composition ratio on properties of  $\text{Cu}_2\text{ZnSnS}_4$  thin films fabricated by co-evaporation. *Thin Solid Films* **518**, S29–S33 (2010)
95. Vora, N., Blackburn, J., Repins, I., Beall, C., To, B., Pankow, J., Teeter, G., Young, M., Noufi, R.: Phase identification and control of thin films deposited by co-evaporation of elemental Cu, Zn, Sn, and Se. *J. Vac. Sci. Technol. A* **30**, 051201 (2012)
96. Weber, A., Krauth, H., Perlt, S., Schubert, B., Kotschau, I., Schorr, S., Schock, H.W.: Multi-stage evaporation of  $\text{Cu}_2\text{ZnSnS}_4$  thin films. *Thin Solid Films* **517**, 2524–2526 (2009)
97. Das, S., Mandal, K.C.: Comparison of  $\text{Cu}_2\text{ZnSnS}_4$  thin film properties prepared by thermal evaporation of elemental metals and binary sulfide sources. In: Photovoltaic Specialists Conference (PVSC), 38th IEEE, Austin, Texas, pp. 002674–002678 (2012)
98. Han, S., Hasoon, S.F., Al-Thani, H.A., Hermann, A.M., Levi, D.H.: Effect of Cu deficiency on the optical properties and electronic structure of  $\text{CuIn}_{1-x}\text{Ga}_x\text{Se}_2$ . *J. Phys. Chem. Solids* **66**, 1895–1898 (2005)
99. Chalapathy, R.B.V., Jung, G.S., Ahn, B.T.: Fabrication of  $\text{Cu}_2\text{ZnSnS}_4$  films by sulfurization of  $\text{Cu/ZnSn/Cu}$  precursor layers in sulfur atmosphere for solar cells. *Sol. Energy Mater. Sol. Cells* **95**, 3216–3221 (2011)
100. Zoppi, G., Forbes, I., Miles, R.W., Dale, P.J., Scragg, J.J., Peter, L.M.:  $\text{Cu}_2\text{ZnSnS}_4$  thin film solar cells produced by selenisation of magnetron sputtered precursors. *Prog. Photovoltaics Res. Appl.* **17**, 315–319 (2009)
101. Momose, N., Htay, M.T., Yudasaka, T., Igarashi, S., Seki, T., Iwano, S., Hashimoto, Y., Ito, K.:  $\text{Cu}_2\text{ZnSnS}_4$  thin film solar cells utilizing sulfurization of metallic precursor prepared by simultaneous sputtering of metal targets. *Jpn. J. Appl. Phys.* **50**, 01BG09 (2011)
102. Fernandes, P.A., Salomé, P.M.P., da Cunha, A.F., Schubert, B.:  $\text{Cu}_2\text{ZnSnS}_4$  solar cells prepared with sulphurized dc-sputtered stacked metallic precursors. *Thin Solid Films* **519**, 7382–7385 (2011)

103. Ito, K., Nakazawa, T.: Proceedings of the 4th international conference on photovoltaics science and engineering, Sydney, Australia, p. 341 (1989)
104. Fernandes, P.A., Salome, P.M.P., da Cunha, A.F.: Precursors' order effect on the properties of sulfurized  $\text{Cu}_2\text{ZnSnS}_4$  thin films. *Semicond. Sci. Technol.* **24**, 105013 (2009)
105. Seol, J.S., Lee, S.Y., Lee, J.C., Nam, H.D., Kim, K.H.: Electrical and optical properties of  $\text{Cu}_2\text{ZnSnS}_4$  thin films prepared by rf magnetron sputtering process. *Sol. Energy Mater. Sol. Cells* **75**, 155–162 (2003)
106. Katagiri, H., Jimbo, K., Tahara, M., Araki, H., Oishi, K.: The influence of the composition ratio on CZTS-based thin film solar cells. In: MRS proceedings, 1165-M04-01 (2009). doi:[10.1557/PROC-1165-M04-01](https://doi.org/10.1557/PROC-1165-M04-01)
107. Yoo, H., Kim, J.: Growth of  $\text{Cu}_2\text{ZnSnS}_4$  thin films using sulfurization of stacked metallic films. *Thin Solid Films* **518**, 6567–6572 (2010)
108. Liu, F., Zhang, K., Lai, Y., Li, J., Zhang, Z., Liu, Y.: Growth and characterization of  $\text{Cu}_2\text{ZnSnS}_4$  thin films by dc reactive magnetron sputtering for photovoltaic applications. *Electrochem. Solid-State Lett.* **13**, H379–H381 (2010)
109. Jimbo, K., Kimura, R., Kamimura, T., Yamada, S., Maw, W.S., Araki, H., Oishi, K., Katagiri, H.:  $\text{Cu}_2\text{ZnSnS}_4$ -type thin film solar cells using abundant materials. *Thin Solid Films* **515**, 5997–5999 (2007)
110. Chrisey, D.B., Hubler, G.K.: Pulsed laser deposition of thin films, vol. 14. Wiley, New York (1994)
111. Sekiguchi, K., Tanaka, K., Moriya, K., Uchiki, H.: Epitaxial growth of  $\text{Cu}_2\text{ZnSnS}_4$  thin films by pulsed laser deposition. *Phys. Status Solidi C* **3**, 2618–2621 (2006)
112. Moriya, K., Tanaka, K., Uchiki, H.: Fabrication of  $\text{Cu}_2\text{ZnSnS}_4$  thin-film solar cell prepared by pulsed laser deposition. *Jpn. J. Appl. Phys.* **46**, 5780–5781 (2007)
113. Moriya, K., Tanaka, K., Uchiki, H.:  $\text{Cu}_2\text{ZnSnS}_4$  thin films annealed in  $\text{H}_2\text{S}$  atmosphere for solar cell absorber prepared by pulsed laser deposition. *Jpn. J. Appl. Phys.* **47**, 602–604 (2008)
114. Pawar, S.M., Moholkar, A.V., Kim, I.K., Shin, S.W., Moon, J.H., Rhee, J.I., Kim, J.H.: Effect of laser incident energy on the structural, morphological and optical properties of  $\text{Cu}_2\text{ZnSnS}_4$  (CZTS) thin films. *Curr. Appl. Phys.* **10**, 565–569 (2010)
115. Sun, L., He, J., Kong, H., Yue, F., Yang, P., Chu, J.: Structure, composition and optical properties of  $\text{Cu}_2\text{ZnSnS}_4$  thin films deposited by pulsed laser deposition method. *Sol. Energy Mater. Sol. Cells* **95**, 2907–2913 (2011)
116. Moholkar, A.V., Shinde, S.S., Babar, A.R., Sim, K., Lee, H., Rajpure, K.Y., Patil, P.S., Bhosale, C.H., Kim, J.H.: Synthesis and characterization of  $\text{Cu}_2\text{ZnSnS}_4$  thin films grown by PLD: solar cells. *J. Alloy. Compd.* **509**, 7439–7446 (2011)
117. Moholkar, A.V., Shinde, S.S., Babar, A.R., Sim, K.-U., Kwon, Y., Rajpure, K.Y., Patil, P.S., Bhosale, C.H., Kim, J.H.: Development of CZTS thin films solar cells by pulsed laser deposition: influence of pulse repetition rate. *Solar Energy* **85**, 1354–1363 (2011)
118. Moholkar, A.V., Shinde, S.S., Agawane, G.L., Jo, S.H., Rajpure, K.Y., Patil, P.S., Bhosale, C.H., Kim, J.H.: Studies of compositional dependent CZTS thin film solar cells by pulsed laser deposition technique: an attempt to improve the efficiency. *J. Alloy. Compd.* **544**, 145–151 (2012)
119. Panthani, M.G., Akhavan, V., Goodfellow, B., Schmidtke, J.P., Dunn, L., Dodabalapur, A., Barbara, P.F., Korgel, B.A.: Synthesis of  $\text{CuInS}_2$ ,  $\text{CuInSe}_2$ , and  $\text{Cu}(\text{In}_{1-x}\text{Ga}_x)\text{Se}_2$  (CIGS) nanocrystal “Inks” for printable photovoltaics. *J. Am. Chem. Soc.* **130**, 16770–16777 (2008)
120. Allen, P.M., Bawendi, M.G.: Ternary I–III–VI quantum dots luminescent in the red to near-infrared. *J. Am. Chem. Soc.* **130**, 9240–9241 (2008)
121. Hernandez-Pagan, E.A., Wang, W., Mallouk, T.E.: Template electrodeposition of single-phase p- and n-type copper indium diselenide ( $\text{CuInSe}_2$ ) nanowire arrays. *ACS Nano* **5**, 3237–3241 (2011)
122. Guo, Q., Kim, S.J., Kar, M., Shafarman, W.N., Birkmire, R.W., Stach, E.A., Agrawal, R., Hillhouse, H.W.: Development of  $\text{CuInSe}_2$  nanocrystal and nanoring inks for low-cost solar cells. *Nano Lett.* **8**, 2982–2987 (2008)

123. Steinhagen, C., Panthani, M.G., Akhavan, V., Goodfellow, B., Koo, B., Korgel, B.A.: Synthesis of  $\text{Cu}_2\text{ZnSnS}_4$  nanocrystals for use in low-cost photovoltaics. *J. Am. Chem. Soc.* **131**, 12554–12555 (2009)
124. Guo, Q., Hillhouse, H.W., Agrawal, R.: Synthesis of  $\text{Cu}_2\text{ZnSnS}_4$  nanocrystal ink and its use for solar cells. *J. Am. Chem. Soc.* **131**, 11672–11673 (2009)
125. Riha, S.C., Parkinson, B.A., Prieto, A.L.: Solution-based synthesis and characterization of  $\text{Cu}_2\text{ZnSnS}_4$  nanocrystals. *J. Am. Chem. Soc.* **131**, 12054–12055 (2009)
126. Cao, Y., Denny Jr, M.S., Caspar, J.V., Farneth, W.E., Guo, Q., Ionkin, A.S., Johnson, L.K., Lu, M., Malajovich, I., Radu, D., Rosenfeld, H.D., Roy, K., Choudhury, W., Wu, W.: High-efficiency solution-processed  $\text{Cu}_2\text{ZnSn}(\text{S},\text{Se})_4$  thin-film solar cells prepared from binary and ternary nanoparticles. *J. Am. Chem. Soc.* **134**, 15644–15647 (2012)
127. Kameyama, T., Osaki, T., Okazaki, K., Shibayama, T., Kudo, A., Kuwabata, S., Torimoto, T.: Preparation and photoelectrochemical properties of densely immobilized  $\text{Cu}_2\text{ZnSnS}_4$  nanoparticle films. *J. Mater. Chem.* **20**, 5319–5324 (2010)
128. Riha, S.C., Fredrick, S.J., Sambur, J.B., Liu, Y., Prieto, A.L., Parkinson, B.A.: Photoelectrochemical characterization of nanocrystalline thin-film  $\text{Cu}_2\text{ZnSnS}_4$  photocathodes. *ACS Appl. Mater. Interfaces* **3**, 58–66 (2011)
129. Shavel, A., Arbiol, J., Cabot, A.: Synthesis of quaternary chalcogenide nanocrystals: stannite  $\text{Cu}_2\text{Zn}_x\text{Sn}_y\text{Se}_{1+x+2y}$ . *J. Am. Chem. Soc.* **132**, 4514–4515 (2010)
130. Lu, X., Zhuang, Z., Peng, Q., Li, Y.: Wurtzite  $\text{Cu}_2\text{ZnSnS}_4$  nanocrystals: a novel quaternary semiconductor. *Chem. Commun.* **47**, 3141–3143 (2011)
131. Dai, P., Shen, X., Lin, Z., Feng, Z., Xu, H., Zhan, J.: Band-gap tunable  $(\text{Cu}_2\text{Sn})_x\text{Zn}_{1-x}\text{S}$  nanoparticles for solar cells. *Chem. Commun.* **46**, 5749–5751 (2010)
132. Cao, M., Shen, Y.: A mild solvothermal route to kesterite quaternary  $\text{Cu}_2\text{ZnSnS}_4$  nanoparticles. *J. Cryst. Growth* **318**, 1117–1120 (2011)
133. Shi, L., Pei, C., Xu, Y., Li, Q.: Template-directed synthesis of ordered single-crystalline nanowires arrays of  $\text{Cu}_2\text{ZnSnS}_4$  and  $\text{Cu}_2\text{ZnSnSe}_4$ . *J. Am. Chem. Soc.* **133**, 10328–10331 (2011)
134. Todorov, T.K., Reuter, K.B., Mitzi, D.B.: High-efficiency solar cell with earth-abundant liquid-processed absorber. *Adv. Mater.* **22**, E156–E159 (2010)
135. Barkhouse, D.A.R., Gunawan, O., Gokmen, T., Todorov, T.K., Mitzi, D.B.: Device characteristics of a 10.1 % hydrazine-processed  $\text{Cu}_2\text{ZnSn}(\text{Se},\text{S})_4$  solar cell. *Prog. Photovoltaics Res. Appl.* **20**, 6–11 (2012)
136. Washio, T., Shinji, T., Tajima, S., Fukano, T., Motohiro, T., Jimbo, K., Katagiri, H.: 6 % efficiency  $\text{Cu}_2\text{ZnSnS}_4$ -based thin film solar cells using oxide precursors by open atmosphere type CVD. *J. Mater. Chem.* **22**, 4021–4024 (2012)
137. Bhattacharya, R.N.: CIGS-based solar cells prepared from electrodeposited stacked Cu/In/Ga layers. *Sol. Energy Materials Solar Cells* **113**, 96–99 (2013)
138. Ahmed, S., Reuter, K.B., Gunawan, O., Guo, L., Romankiw, L.T., Deligianni, H.: A high efficiency electrodeposited  $\text{Cu}_2\text{ZnSnS}_4$  solar cell. *Adv. Energy Mater.* **2**, 253–259 (2012)
139. Ennaoui, A., Steiner, M.L., Weber, A., Ras, D.A., Kotschau, I., Schock, H.W., Schurr, R., Holzinger, A., Jost, S., Hock, R., Vob, T., Schulze, J., Kirbs, A.:  $\text{Cu}_2\text{ZnSnS}_4$  thin film solar cells from electrodeposited precursors: novel low-cost perspective. *Thin Solid Films* **517**, 2511–2514 (2009)
140. Araki, H., Kubo, Y., Jimbo, K., Maw, W.S., Katagiri, H., Yamazaki, M., Oishi, K., Takeuchi, A.: Preparation of  $\text{Cu}_2\text{ZnSnS}_4$  thin films by sulfurization of co-electroplated Cu–Zn–Sn precursors. *Phys. Status Solidi C* **6**, 1266–1268 (2009)
141. Kurihara, M., Berg, D., Fisher, J., Siebentritt, S., Dale, P.J.: Kesterite absorber layer uniformity from electrodeposited precursors. *Phys. Status Solidi C* **6**, 1241–1244 (2009)
142. Pawar, S.M., Pawar, B.S., Moholkar, A.V., Choi, D.S., Yun, J.H., Moon, J.H., Kolekar, S.S., Kim, J.H.: Single step electrosynthesis of  $\text{Cu}_2\text{ZnSnS}_4$  (CZTS) thin films for solar cell application. *Electrochim. Acta* **55**, 4057–4061 (2010)
143. Chan, C.P., Lam, H., Surya, C.: Preparation of  $\text{Cu}_2\text{ZnSnS}_4$  films by electrodeposition using ionic liquids. *Sol. Energy Mater. Sol. Cells* **94**, 207–211 (2010)



144. Schurr, R., Hölzing, A., Jost, S., Hock, R., Voß, T., Schulze, J., Kirbs, A., Ennaoui, A., Lux-Steiner, M., Weber, A., Kötschau, I., Schock, H.-W.: The crystallisation of  $\text{Cu}_2\text{ZnSnS}_4$  thin film solar cell absorbers from co-electroplated Cu–Zn–Sn precursors. *Thin Solid Films* **517**, 2465–2468 (2009)
145. Bhattacharya, R.N.: Fabrication of ionic liquid electrodeposited Cu–Sn–Zn–S–Se thin films and method of making, United States Patent Application Publication No.: US 2013/0168825 A1, July 4, 2013
146. Farinella, M., Inguanta, R., Spano, T., Livreri, P., Piazza, S., Sunseri, C.: Electrochemical deposition of CZTS thin films on flexible substrate. *Energy Procedia* **44**, 105–110 (2014)
147. Bhattacharya, R.N.: 3.6 %-CZTSS Device fabricated from ionic liquid electrodeposited Sn layer. *Open Surface Sci. J.* **5**, 21–24 (2013)
148. Timmo, K., Altosaar, M., Raudoja, J., Muska, K., Pilvet, M., Kauk, M., Varema, T., Danilson, M., Volobujeva, O., Mellikov, E.: Sulfur-containing  $\text{Cu}_2\text{ZnSnSe}_4$  monograin powders for solar cells. *Sol. Energy Mater. Sol. Cells* **94**, 1889–1892 (2010)
149. Mellikov, E., Meissner, D., Varema, T., Altosaar, M., Kauk, M., Volobujeva, O., Raudoja, J., Timmo, K., Danilson, M.: Monograin materials for solar cells. *Sol. Energy Mater. Sol. Cells* **93**, 65–68 (2009)
150. Kauk, M., Muska, K., Altosaar, M., Raudoja, J., Pilvet, M., Varema, T., Timmo, K., Volobujeva, O.: Effects of sulphur and tin disulphide vapour treatments of  $\text{Cu}_2\text{ZnSnS}(\text{Se})_4$  absorber materials for monograin solar cells. *Energy Procedia* **10**, 197–202 (2011)
151. Katagiri, H.:  $\text{Cu}_2\text{ZnSnS}_4$  thin film solar cells. *Thin Solid Films* **480–481**, 426–432 (2005)
152. Jeong, A.R., Jo, W., Jung, S., Gwak, J., Yun, J.H.: Enhanced exciton separation through negative energy band bending at grain boundaries of  $\text{Cu}_2\text{ZnSnSe}_4$  thin-films. *Appl. Phys. Lett.* **99**, 082103 (2011)
153. Shin, B., Wang, K., Gunawan, O., Reuter, K.B., Chey, S.J., Bojarczuk, N.A., Todorov, T., Mitzi, D.B., Guha, S.: Photovoltaic specialists conference (PVSC), 37th IEEE (2011), pp. 002510–002514
154. Jung, S., Gwak, J., Yun, J.H., Ahn, S.J., Nam, D., Cheong, H., Ahn, S., Cho, A., Shin, K.S., Yoon, K.H.:  $\text{Cu}_2\text{ZnSnSe}_4$  thin film solar cells based on a single-step co-evaporation process. *Thin Solid Films* **535**, 52–56 (2013)
155. Platzer-Björkman, C., Scragg, J., Flammersberger, H., Kubart, T., Edoff, M.: Influence of precursor sulfur content on film formation and compositional changes in  $\text{Cu}_2\text{ZnSnS}_4$  films and solar cells. *Solar Energy Materials and Solar Cells* **98**, 110–117 (2012)
156. Ericson, T., Scragg, J.J., Kubart, T., Törndahl, T., Platzer-Björkman, C.: Annealing behavior of reactively sputtered precursor films for  $\text{Cu}_2\text{ZnSnS}_4$  solar cells. *Thin Solid Films* **535**, 22–26 (2013)
157. Lechner, R., Jost, S., Palm, J., Gowtham, M., Sorin, F., Louis, B., Yoo, H., Wibowo, R.A., Hock, R.:  $\text{Cu}_2\text{ZnSn}(\text{S}, \text{Se})_4$  solar cells processed by rapid thermal processing of stacked elemental layer precursors. *Thin Solid Films* **535**, 5–9 (2013)
158. Woo, K., Kim, Y., Moon, J.: A non-toxic, solution-processed, earth abundant absorbing layer for thin-film solar cells. *Energy Environ. Sci.* **5**, 5340–5345 (2012)
159. Ki, W., Hillhouse, H.W.: Earth-abundant element photovoltaics directly from soluble precursors with high yield using a non-toxic solvent. *Adv. Energy Mater.* **1**, 732–735 (2011)
160. Ford, G.M., Guo, Q., Agrawal, R., Hillhouse, H.W.: Earth abundant element  $\text{Cu}_2\text{Zn}(\text{Sn}_{1-x}\text{Ge}_x)\text{S}_4$  nanocrystals for tunable band gap solar cells: 6.8 % efficient device fabrication. *Chem. Mater.* **23**, 2626–2629 (2011)
161. Maeda, K., Tanaka, K., Fukui, Y., Uchiki, H.: Influence of  $\text{H}_2\text{S}$  concentration on the properties of  $\text{Cu}_2\text{ZnSnS}_4$  thin films and solar cells prepared by sol–gel sulfurization. *Sol. Energy Mater. Sol. Cells* **95**, 2855–2860 (2011)
162. Tanaka, K., Fukui, Y., Moritake, N., Uchiki, H.: Chemical composition dependence of morphological and optical properties of  $\text{Cu}_2\text{ZnSnS}_4$  thin films deposited by sol–gel sulfurization and  $\text{Cu}_2\text{ZnSnS}_4$  thin film solar cell efficiency. *Sol. Energy Mater. Sol. Cells* **95**, 838–842 (2011)

163. Moritake, N., Fukui, Y., Oonuki, M., Tanaka, K., Uchiki, H.: Preparation of  $\text{Cu}_2\text{ZnSnS}_4$  thin film solar cells under non-vacuum condition. *Phys. Status Solidi C* **6**, 1233–1236 (2009)
164. Tanaka, K., Oonuki, M., Moritake, N., Uchiki, H.:  $\text{Cu}_2\text{ZnSnS}_4$  thin film solar cells prepared by non-vacuum processing. *Sol. Energy Mater. Sol. Cells* **93**, 583–587 (2009)
165. Jiang, M., Li, Y., Dhakal, R., Thapaliya, P., Mastro, M., Caldwell, J.D., Kub, F., Yan, X.:  $\text{Cu}_2\text{ZnSnS}_4$  polycrystalline thin films with large densely packed grains prepared by sol-gel method. *J. Photonics Energy* **1**, 019501 (2011)
166. Ilari, G.M., Fella, C.M., Ziegler, C., Uhl, A.R., Romanyuk, Y.E., Tiwari, A.N.:  $\text{Cu}_2\text{ZnSnSe}_4$  solar cell absorbers spin-coated from amine-containing ether solutions. *Sol. Energy Mater. Sol. Cells* **104**, 125–130 (2012)
167. Zhou, Z., Wang, Y., Xu, D., Zhang, Y.: Fabrication of  $\text{Cu}_2\text{ZnSnS}_4$  screen printed layers for solar cells. *Sol. Energy Mater. Sol. Cells* **94**, 2042–2045 (2010)
168. Chen, Q., Cheng, S., Zhuang, S., Dou, X.:  $\text{Cu}_2\text{ZnSnS}_4$  solar cell prepared entirely by non-vacuum processes. *Thin Solid Films* **520**, 6256–6261 (2012)
169. Prabhakar, T., Nagaraju, J.: Device parameters of  $\text{Cu}_2\text{ZnSnS}_4$  thin film solar cell. Photovoltaic Specialists Conference (PVSC), 37th IEEE, Seattle, pp. 001346–001351 (2011)
170. Patel, M., Mukhopadhyay, I., Ray, A.: Structural, optical and electrical properties of spray-deposited CZTS thin films under a non-equilibrium growth condition. *J. Phys. D Appl. Phys.* **45**, 445103 (2012)
171. Wangperawong, A., King, J.S., Herron, S.M., Tran, B.P., Pangan-Okimoto, K., Bent, S.F.: Aqueous bath process for deposition of  $\text{Cu}_2\text{ZnSnS}_4$  photovoltaic absorbers. *Thin Solid Films* **519**, 2488–2492 (2011)